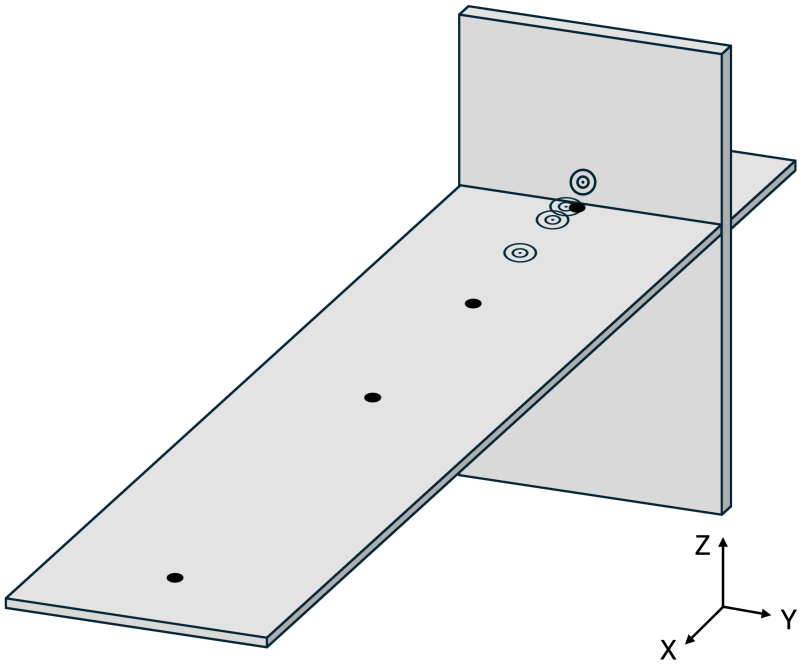

Theory and Measurement of Low-Frequency Structure-Borne Sound in Concrete Buildings

Structural Vibration Analysis of a Concrete Floor

Master's thesis in Master's Programme in Sound and Vibration

JIALI CHENG

DEPARTMENT OF ARCHITECTURE AND CIVIL ENGINEERING

CHALMERS UNIVERSITY OF TECHNOLOGY
Gothenburg, Sweden 2025
www.chalmers.se

Master's thesis 2025

Theory and Measurement of Low-Frequency Structure-Borne Sound in Concrete Buildings

Structural Vibration Analysis of a Concrete Floor

JIALI CHENG

CHALMERS
UNIVERSITY OF TECHNOLOGY

Department of Architecture and Civil Engineering
Division of Applied Acoustics
Chalmers University of Technology
Gothenburg, Sweden 2025

Theory and Measurement of Low-Frequency Structure-Borne Sound in Concrete Buildings
Structural Vibration Analysis of a Concrete Floor
JIALI CHENG

Industrial Supervisors: Magne Skålevik, Brekke & Strand Akustikk AS
Kjetil Vedholm, Brekke & Strand Akustik AB

Supervisor & Examiner: Jens Forssén, Division of Applied Acoustics
Chalmers University of Technology

Master's Thesis 2025
Department of Architecture and Civil Engineering
Division of Applied Acoustics
Chalmers University of Technology
SE-412 96 Gothenburg
Telephone +46 31 772 1000

Cover: Measurement setup for structural vibrations of a concrete floor, showing excitation and measurement positions, sketched using Microsoft PowerPoint.

Typeset in LaTeX
Printed by Chalmers Reproservice
Gothenburg, Sweden 2025

Theory and Measurement of Low-Frequency Structure-Borne Sound in Concrete Buildings
Structural Vibration Analysis of a Concrete Floor
JIALI CHENG
Department of Architecture and Civil Engineering
Chalmers University of Technology

Abstract

Low-frequency structure-borne sound is a critical issue because this type of noise travels long distances with little attenuation. This has become a growing concern with the advancement of audio technology and loudspeakers. It is especially problematic in spaces like home theatres and concert halls, where it can cause discomfort and long-term health effects for residents, even those located at a distance. Therefore, predicting effective sound insulation in the early building design process is essential. This thesis investigates the behaviour of low-frequency vibrations in a concrete floor within an office building, focusing on the relationship between the propagation speed of bending waves, the loss factor, and the attenuation of vibrations over distance. It is built on the work of Østvik[1], who described the correlation between structural reverberation and distance-dependent damping of vibrations of a concrete slab within a building.

A theoretical model of vibration decay, based on the propagation speed and the loss factor of the structure, was proposed and validated through vibration measurements. These measurements were conducted at multiple excitation points on both the floor and the wall, with results confirming that the propagation speed of bending waves follows the expected square-root dependence on frequency. A lower propagation speed was observed when the floor was excited on the wall, compared to direct excitations on the floor. The level decay predicted by the model generally followed a logarithmic pattern, with geometric spreading being dominant. More significant decay was observed at higher frequencies than at lower ones. Furthermore, the structural reverberation time was found to decrease with increasing frequency, indicating that the vibrations last longer at low frequencies. The total loss factor also decreased with increasing frequency, suggesting that energy loss per oscillation is greater at low frequencies. These findings provide valuable insights into low-frequency vibration propagation. Further research with additional excitation and measurement positions is needed to validate the proposed relationship and better understand the variations observed in this study.

Keywords: low-frequency sound, structure-borne sound, concrete, structural analysis, bending waves, time delay, level decay, distance attenuation, structural reverberation time, loss factor.

[1]L. Østvik, "Utbredelse av strukturlyd i større bygninger i betong. En måleoppgave.," NTNU, Trondheim, Trøndelag, Norway, Rep. Dec. 2018.

Acknowledgements

This thesis topic was proposed by Magne Skålevik from Brekke & Strand Akustikk AS, and the measurements were carried out in collaboration with Kjetil Vedholm from Brekke & Strand Akustik AB. The work is built upon the contributions of Live Østvik, whose previous research laid the foundation for this study.

First and foremost, I would like to thank my supervisors, Magne Skålevik, Kjetil Vedholm, and Jens Forssén, for the opportunity to carry out this project. I am especially grateful to Magne for his vision in shaping the direction of this project, to Kjetil for coordinating measurements outside office hours, and to Jens for his endless patience and support. I truly appreciate their expertise, guidance, and feedback throughout the thesis work, which have been invaluable to me. A special thank-you to Jens Forssén, who is also my examiner, for his thoughtful input and constructive feedback on my thesis.

I would like to extend my thanks to my colleagues and all the staff in the Sound and Vibration master's program at the Division of Applied Acoustics, Chalmers University of Technology. Their support, encouragement, and expertise in the field have been essential to the completion of this thesis. These two and half years have been a wonderful experience for me as an international student in Sweden.

Lastly, I would also like to thank my friends for their constant encouragement, and I express my deepest gratitude to my family, who have supported and trusted me unconditionally throughout this journey.

This thesis would not have been possible without their support. Thank you for everything! ♡

Jiali Cheng
Gothenburg, November 2024

AI Disclosure Statement

During the preparation of this work, the author used OpenAI ChatGPT in the following aspects:

- Debugging scripts and formatting plots in MATLAB
- Debugging and formatting in Overleaf
- Grammar and spelling checks

After using this tool, the author reviewed and edited the content as needed, and takes full responsibility for the content of the publication.

List of Acronyms

Below is the list of acronyms that have been used throughout this thesis listed in alphabetical order:

CLF	Coupling Loss Factor
ESD	Energy Spectral Density
FDTD	Finite-Difference Time-Domain Method
FEA	Finite Element Analysis
FFT	Fast Fourier Transform
SBN	Structure-Borne Noise
SEA	Statistical Energy Analysis

Nomenclature

Below is the nomenclature of constants, indices, parameters, and variables that have been used throughout this thesis.

Constants

e	Euler's number
j	$\sqrt{-1}$
π	Pi, the ratio of a circle's circumference to its diameter

Indices

a,b,c	Indices for specific time points
x,y,z	Indices for spatial positions

Parameters

a	Acceleration
c	Speed
c_0	Speed of sound in air
c_B	Bending wave propagation speed
c_gB	Group velocity of bending waves
c_ph	Phase velocity
η	Displacement
$\mathsf{\eta}$	Loss factor
$\mathsf{\eta}_\mathrm{int}$	Internal loss factor
$\mathsf{\eta}_\mathrm{tot}$	Total loss factor
f	Frequency

f_c	Critical frequency
k	Wave number
λ	Wavelength
m	Mass per unit length or area
ν	Poisson's ratio
ρ	Density
ρ_0	Density of air
σ	Radiation efficiency
t	Time
t_s	Centre time (centre of gravity time)
τ	Time delay
u, v	Velocity
φ	Phase angle
ω	Angular frequency
B	Bending stiffness
E	Young's modulus (modulus of elasticity)
E_{tot}	Total vibration (velocity or acceleration) energy
I	Moment of inertia
R^2	Coefficient of determination
$R_{xy}(\tau)$	Cross-correlation function
S	Area
T_{60}	Reverberation time
T_s	Structural reverberation time
W	Sound power

Variables

b	Cross-sectional width
d	Slope of the linear fit
h	Thickness
r	Distance
D_{B}	Vibration level decay in dB/m
L	Vibration level in dB

Contents

List of Figures

List of Tables

1
Introduction

1.1 Background

With advancements in audio technology, audio devices such as loudspeakers have become increasingly accessible. Subwoofers, which are loudspeakers specifically designed to produce deep bass sound in the range of 20 Hz to 200 Hz, are particularly noteworthy. These low-frequency sounds can excite structures such as walls and floors, leading to vibrations that radiate audible sounds. This type of noise can travel long distances with little attenuation, and ear protection devices often fail to provide adequate shielding [1]. It can induce prolonged stress in humans and cause chronic psychophysiological damage under long-term exposure [2]. This phenomenon is critical in spaces like home theatres, music venues, and concert halls, where disturbance can be high. Therefore, predicting practical sound insulation during the early stages of building development is crucial. However, the understanding of this problem is underdeveloped due to its complex nature.

Gjesland [3] reviewed current building codes and regulations on low-frequency sound insulation in buildings, noting that specifications for handling sound below 50 Hz are rarely included. Sadeghi and Vasheghani [4] also pointed out that no current building codes have included structure-borne noise as a criterion in the design of buildings. This thesis builds upon the work of Østvik [5], who investigated the correlation between structural reverberation and distance damping of vibrations of a concrete slab within a building.

1.2 Problem Formulation

Sound can be generated by vibrating bodies that disturb the surrounding air, causing local fluctuations in air pressure [6]. Expressions for radiated power from a vibrating surface can be found in acoustics books and standards, such as in [7], [8], and [9]:

$$W = \rho_0 c_0 S \overline{|v|^2} \sigma \tag{1.1}$$

where S is the area of the vibrating surface, ρ_0 is the density of the air, c_0 is the speed of the sound in air, ($\rho_0 c_0$ is the characteristic impedance of air), $\overline{|v|^2}$ is the spatially averaged, mean-square velocity that is normal to the surface, and σ is radiation efficiency. σ can be assumed to be 1 above the critical frequency. Since parameters

S, ρ, and c are constants, accurately estimating $\overline{|v|^2}$ - the vibration amplitude as a function of frequency and its spatial distribution - as well as the radiation efficiency σ of vibrating surfaces allows for the prediction of radiated power W.

This thesis focuses on vibration propagation in plates in terms of the propagation speed and distance attenuation of vibrations normal to the surface, and structural reverberation time. According to Østvik [5], it was found that the reverberation time slightly increases with distance for low-frequency bands at short distances, then decreases at distances greater than 6 metres. Additionally, the time delay was found to increase linearly with distance, with an average propagation speed of 833 m/s and a distance attenuation of 8.84 dB/m for distances greater than 7 metres.

1.3 Aim and Objectives

This thesis aims to develop an understanding of the structural vibration of concrete slabs in an office building through measurements and analysis. The following questions will be investigated:

- Test the model and hypothesis presented in Østvik's report.
  - Is there a significant relationship between the temporal decay and the attenuation over distance for velocities in a building structure, measured within the same octave band?
    - Can this relationship be predicted?
    - Is it related to the propagation speed of waves in structures?

1.4 Limitations

Due to constraints related to time, location, and the scope of existing knowledge on the topic, this thesis will focus exclusively on the structural vibrations of a single concrete floor in an office building in Gothenburg, Sweden. The excitation source was a kettlebell due to the limited availability of equipment at the time of measurement.

1.5 Outline of Thesis

The thesis is structured as follows: Chapter 2 briefly introduces the terminologies and fundamental theories necessary to understand low-frequency sound and structural vibrations. The measurement setup and evaluation method are detailed in Chapter 3. Chapter 4 presents and discusses the results, while Chapter 5 provides the conclusions drawn from the study.

2

Theory

As stated in Chapter 1, this thesis focuses on the vibration mechanism in plates in terms of the propagation speed and distance attenuation of vibrations perpendicular to the surface, and structural reverberation time, as "only motions perpendicular to a surface can cause radiation of sound into an adjacent medium" [7, pp. 35]. Cremer, Heckl, and Petersson detail the wave types and their characteristics in *Structure-Borne Sound* [7], showing that bending waves, or so-called flexural waves, contribute most to sound radiation due to their unique behaviours compared with longitudinal waves and transverse waves. Hence only a brief summary of bending waves in beams and plates is provided here.

2.1 Bending Waves in Beams and Plates

Bending waves or flexural waves are a hybrid between shear and longitudinal waves. They cause both rotation and lateral displacement of the beam or plate elements. Their greatest importance in sound radiation is due to their significant lateral deflections and similar transverse impedance as that of sound waves in the surrounding air [8, pp. 19]. Assuming the plane wave travels in an infinitely long uniform beam or an infinitely large flat isotropic plate (undamped) in the x direction, the bending motion can be characterized by

$$B\frac{\partial^4 \eta}{\partial x^4} = -m\frac{\partial^2 \eta}{\partial t^2}, \tag{2.1}$$

with η defined as the displacement in the direction normal to the plate surface, B is the bending stiffness and m is the mass per unit length for beams and mass per unit area for plates.

By substituting a simple harmonic wave $\eta(x,t) = \widetilde{\eta}e^{j(\omega t - kx)}$ in which ω is the angular frequency (phase change per unit time) and k is the wave number ($k = \omega/c_{\text{ph}} = 2\pi/\lambda$, with c_{ph} the phase velocity and λ the wavelength), Eq. 2.1 becomes

$$Bk^4 = \omega^2 m, \tag{2.2}$$

and the free wave solution is thus

$$\eta(x,t) = (\eta_+ e^{-jk_b x} + \eta_- e^{jk_b x} + \eta_{j+} e^{-k_b x} + \eta_{j-} e^{k_b x})e^{-j\omega t}, \tag{2.3}$$

where $k_b = (\omega^2 m/B)^{1/4}$. The first two terms of the free wave solution indicate waves propagating in the x directions, and the second two terms denote the "near fields", or "evanescent waves" in many literature, as they have imaginary phase velocities and thus do not transport energy.

2.1.1 Propagation Speed

Eq. 2.3 yields the phase speed of the waves propagating in the x directions,

$$c_{\mathrm{B}} = \frac{\omega}{k_b} = \omega^{\frac{1}{2}}(\frac{B}{m})^{\frac{1}{4}} = (\omega^2 \frac{B}{m})^{\frac{1}{4}}. \tag{2.4}$$

Its dependency on frequency ($c_{\mathrm{B}} \propto w^{1/2}$) makes bending waves dispersive, with a group velocity (for one-dimensional case such as a beam):

$$c_{\mathrm{gB}} = \frac{d\omega}{dk} = 2c_{\mathrm{B}}. \tag{2.5}$$

The group velocity represents the speed at which energy is transported. For two- or three-dimensional cases, this velocity is lower, as energy is spread over a larger area. The dispersive nature of bending waves implies that their natural frequencies are not harmonically related.

Table 2.1 shows the equations for beams and plates when substituting variables in Eq. 2.4, where E is Young's modulus or modulus of elasticity, I is the second moment of area, ν is the Poisson's ratio, ρ is the density of the structure material, h is the thickness of the beam or plate, and b is the rectangular cross-section width. Note that the variable b is cancelled out when plugging equations for beams in Eq. 2.4, and thus the speed only differs by $(1-\nu^2)^{-1/4}$ between beams and plates.

	B	I	m	c_{B}
beam	EI	$\frac{bh^3}{12}$	ρbh	$(\omega^2 \frac{Eh^2}{12\rho})^{1/4}$
plate	$\frac{EI}{1-\nu^2}$	$\frac{h^3}{12}$	ρh	$(\omega^2 \frac{Eh^2}{12(1-\nu^2)\rho})^{1/4}$

Table 2.1: Equations for beams and plates.

It is worth noting that the assumption in Eq. 2.1 neglects the shear distortion to the transverse displacement of bending waves, which holds if the bending wavelength is greater than $6h$ ($\lambda_{\mathrm{B}} > 6h$), i.e. at low frequencies. At higher frequencies ($\lambda_{\mathrm{B}} < 6h$), a corrected wave speed according to Cremer, Heckl, and Petersson [7, pp. 126] is approximated by

$$c_{\mathrm{C}} \approx c_{\mathrm{B}}[1 - 4(\frac{h}{\lambda_{\mathrm{B}}})^2]. \tag{2.6}$$

It is obvious that the corrected wave speed is smaller than the uncorrected one ($c_{\mathrm{C}} < c_{\mathrm{B}}$). An example illustration of bending waves phase speeds of a 270-mm

thick concrete slab using Eq. 2.4 and Eq. 2.6 is shown in Figure 2.1. The concrete properties E, ρ, and ν are estimated reference to [7, pp. 196], [8, pp. 15], and [10]. The $6h$ limit is about 500 Hz for such a structure. The deviation between corrected and uncorrected terms is about 10 % at this frequency. Equations for a beam and a plate give very close results, as expected due to the $(1-\nu^2)^{-1/4}$ difference, with the propagation speed in a plate 1 % higher than that of a beam. In this case, it is sufficient to model a beam or a plate using uncorrected terms for frequencies lower than 500 Hz.

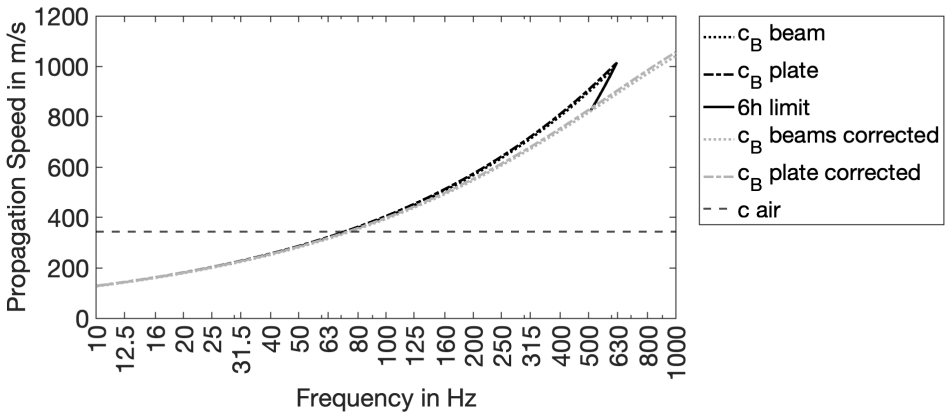

Figure 2.1: Propagation speed of bending waves in a 270-mm thick concrete slab, using equations for beams and plates. The concrete properties are: $E = 26\,\mathrm{GPa}$, $\rho = 2400\,\mathrm{m/s^2}$, $\nu = 0.2$.

The phase speed of bending waves in the structure at a certain frequency is identical to the speed of sound in the surrounding medium (e.g. air). It is called the critical frequency f_c, or the lowest coincidence frequency, and is given by

$$f_c = \frac{c_0^2}{2\pi}\sqrt{\frac{m}{B}}, \tag{2.7}$$

with c_0 denoting the speed in air, which is approximately 343 m/s at 20 °C. The critical frequency increases with increasing mass and decreasing bending stiffness. For a structure in Figure 2.1, the critical frequency is about 70 Hz. For $f < f_c$ or $\lambda_\mathrm{B} < \lambda$, no sound radiates for ideal infinite structures. The radiation efficiency is infinity at the critical frequency and goes towards 1 above that. For real finite structures, it would depend on the length of the edge and boundary conditions. A significant reduction in the radiation would happen below the critical frequency due to the hydrodynamic short-circuit effect, and strong radiation above f_c with directionality effect [7].

2.1.2 Damping & Level Decay

The equations illustrated in the previous section (section 2.1.1) describe an ideal undamped situation. In real life, the mechanical energy dissipates and converts into

heat, resulting in a phase difference between stress and strain [7, pp. 153]. By introducing an internal loss factor η, the complex Young's modulus is

$$\underline{E} = E' + jE'' = E'(1 + j\eta), \tag{2.8}$$

with $\eta = E''/E'$. For weak damping ($\eta << 1$) and pure bending waves, Eq. 2.4 becomes

$$\underline{c}_{\mathrm{B}} = \omega^{\frac{1}{2}}(\frac{B'(1+j\eta)}{m})^{\frac{1}{4}} \approx \omega^{\frac{1}{2}}(\frac{B'}{m})^{\frac{1}{4}}(1 + j\frac{\eta}{4}) = c'_{\mathrm{B}}(1 + j\frac{\eta}{4}). \tag{2.9}$$

The corresponding wavenumber ($\underline{k} = k' - jk''$) is then

$$\underline{k}_{\mathrm{B}} = \frac{\omega}{\underline{c}_{\mathrm{B}}} \approx (\omega^2\frac{m}{B'})^{\frac{1}{4}}(1 - j\frac{\eta}{4}) = k'_{\mathrm{B}}(1 - j\frac{\eta}{4}). \tag{2.10}$$

The approximation is from Taylor expansion. For beams in which $c_{\mathrm{gB}} = 2c_{\mathrm{B}}$, the imaginary part of wavenumber can be written as

$$k''_{\mathrm{B}} \approx \frac{\pi\eta}{2\lambda_{\mathrm{B}}} = \frac{\pi\eta f}{2c_{\mathrm{B}}} = \frac{\pi\eta f}{c_{\mathrm{gB}}}. \tag{2.11}$$

Assuming plane waves propagating in the positive x direction [7, pp. 156], with velocity (or acceleration)

$$u(x,t) = \mathrm{Re}\{\hat{u}e^{j(\omega t - \underline{k}_{\mathrm{B}}x)}\} = \hat{u}e^{-k''x}\cos(\omega t - k'x + \varphi), \tag{2.12}$$

which implies that the amplitude decays exponentially by a factor of $e^{-\pi\eta/2}$ within a wavelength. The level decay of vibration (velocity or acceleration) with distance for bending waves then follows

$$\Delta L_{\mathrm{B}} = 20\log_{10}(e^{k''\Delta x}) = \frac{10}{\ln(10)}\frac{\omega\eta\Delta x}{2c_{\mathrm{B}}} \approx \frac{4.34\pi\eta\Delta x}{\lambda_{\mathrm{B}}}\ (\mathrm{dB}). \tag{2.13}$$

The level decay in (dB/m) is therefore

$$D_{\mathrm{B}} = \frac{\Delta L_{\mathrm{B}}}{\Delta x} \approx 13.64\frac{\eta}{\lambda_{\mathrm{B}}}\ (\mathrm{dB/m}). \tag{2.14}$$

Assuming a constant internal loss factor of $6 \cdot 10^{-3}$ as in concrete [7, pp. 196] [11], a structure as stated in Figure 2.1 follows a decay as illustrated in Figure 2.2. The calculation was computed in distance from 0 to 20 metres and frequency below 500 Hz. The wave speed of a beam was used.

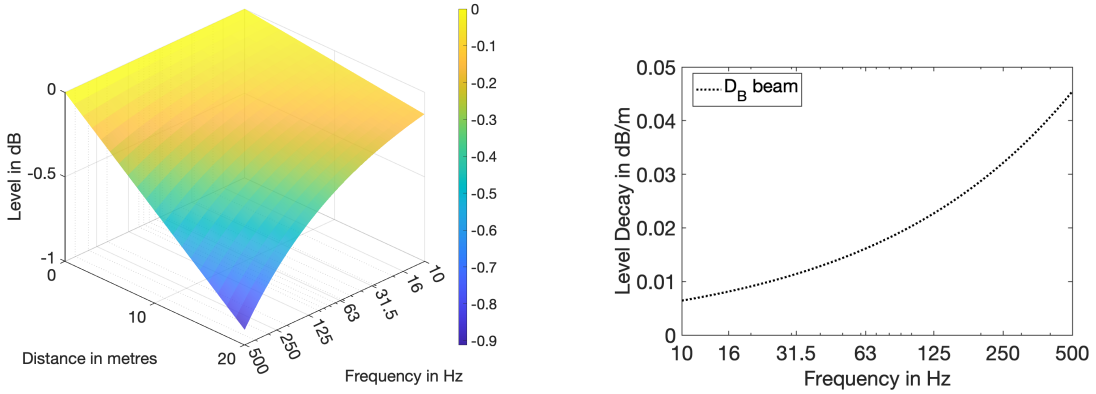

(a) L_B in dB as a function of distance and frequency reference to $L_\mathrm{B}(x = 0)$.

(b) D_B in dB/m as a function of frequency.

Figure 2.2: Vibration level decay of free bending waves in a beam due to material damping, with a constant internal loss factor η_int of $6 \cdot 10^{-3}$ and structural properties stated in Figure 2.1.

It can be seen from Figure 2.2a that lower frequencies damped less due to their long wavelengths compared with higher frequencies, which is illustrated in Figure 2.2b. The level decay in (dB/m) at 500 Hz is roughly 6 times greater than that of at 10 Hz, or the level decay at 10 Hz is nearly 86 % less than that of at 500 Hz.

In addition to material damping, the vibration level will decay with distance r in the two-dimensional case (i.e. in a plate) according to the distance law [12, pp. 253]. A cylindrical wave radiates out from the excitation position, and attenuation with distance occurs due to both geometrical spreading of the wavefront and internal damping [13]. As for the three-dimensional case, the energy decays with r^2 with spherical propagation [14, 15]. With geometrical spreading added to the material damping, the vibration level at distances $r \geq 1\,\mathrm{m}$ relative to $L_\mathrm{B}(r = 0)$ is then

$$L_\mathrm{B}(r) \approx -N \log_{10}(r) - \frac{4.34\pi\eta}{\lambda_\mathrm{B}} r, \tag{2.15}$$

with $N = 10$ for 2D and $N = 20$ for 3D. The decrease in vibration level in (dB/m) is thus

$$D_\mathrm{B}(r) = -\frac{dL_\mathrm{B}}{dr} \approx \frac{N}{\ln(10) r} + \frac{4.34\pi\eta}{\lambda_\mathrm{B}}. \tag{2.16}$$

Figure 2.3 illustrates the vibration level in dB and the decrease in dB/m reference to $r = 0$ for a plate (with properties stated in Figure 2.1) as a function of distance from 1 metre to 20 metres and frequency from 0 Hz to 500 Hz. The internal loss factor used was the same as in Figure 2.2, with the left figure showing the 3-D view and the right figure showing the same with a different angle (along the axis of distance).

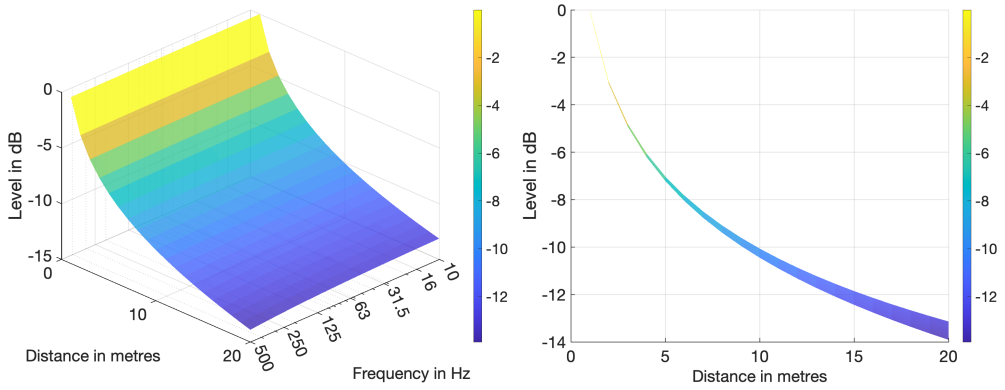

(a) L_{B}.

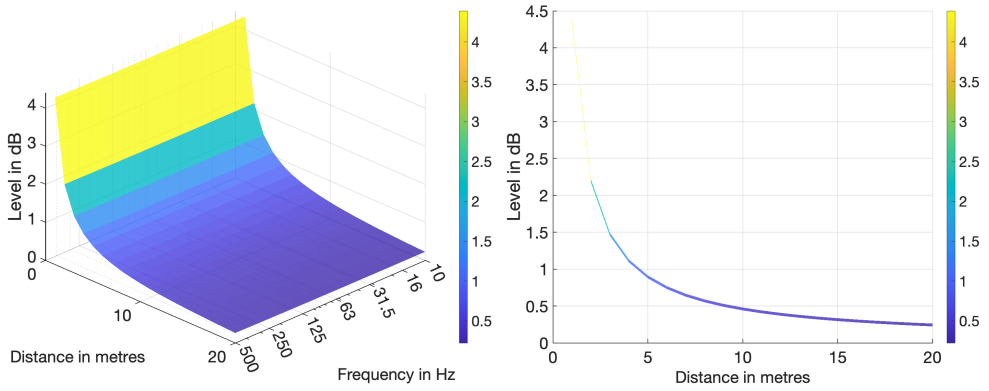

(b) D_{B}.

Figure 2.3: L_{B} in dB and D_{B} in dB/m for a plate due to geometrical spreading and material damping as a function of distance and frequency reference to $r = 0$, with $\eta_{\mathrm{int}} = 6 \cdot 10^{-3}$ and structural properties stated in Figure 2.1.

The calculations so far assume an infinite beam or plate and a direct or nonresonant wave is present. It is obvious that geometrical spreading contributes dominantly to the decay of the direct wave, and material damping has small effects, especially at short distances. The loss factor η must be very large to substantially influence the direct wave decay. As an example, a constant loss factor of 0.05 and 0.1 was applied to the same structure, shown in Figure 2.4a and Figure 2.4b respectively, to see the effects.

With the loss factor increases from 10^{-3} as in Figure 2.3a to 10^{-2} and 10^{-1} as in Figure 2.4, the vibration level varies more between lower and higher frequencies, and the difference increases as the waves propagate further away. For example, at very low frequencies, such as 10 Hz, the vibration level at 20 m increases by approximately 7 % for $\eta \approx 10^{-2}$ and 15 % for $\eta \approx 10^{-1}$, compared with the level with $\eta \approx 10^{-3}$ at the same distance; while for higher frequencies like 500 Hz, the increment is 48 % and 102 %, respectively.

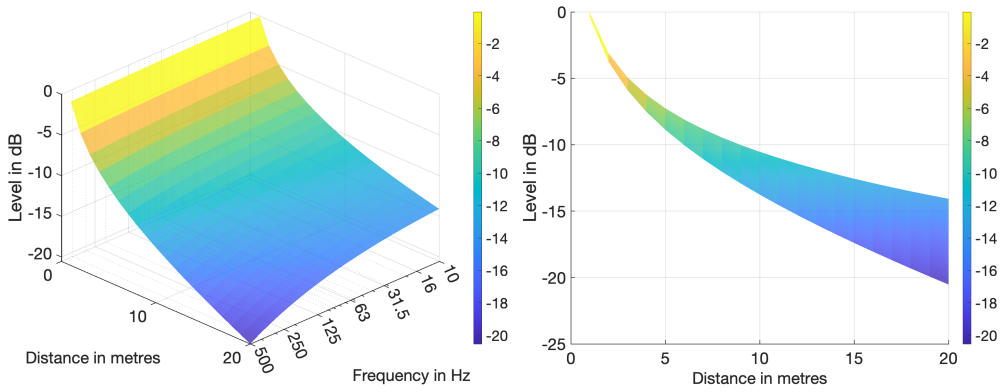

(a) $\eta = 0.05$.

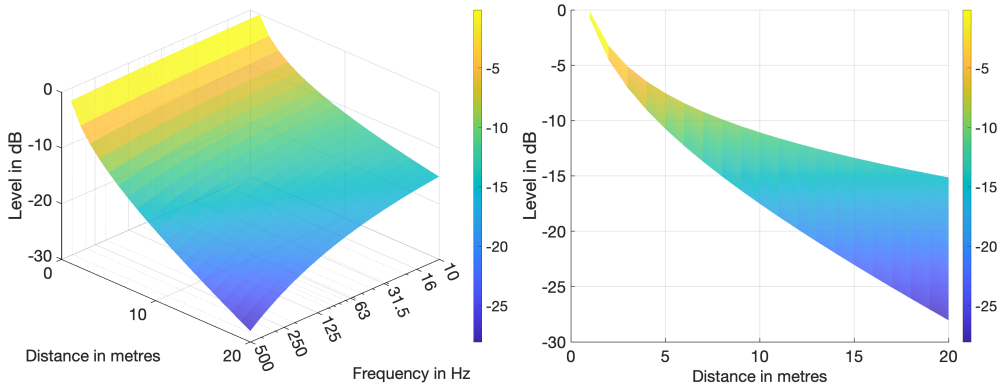

(b) $\eta = 0.1$.

Figure 2.4: L_B in a plate in dB due to geometrical spreading and material damping as a function of distance and frequency reference to $L_B(r = 0)$, with (a) $\eta = 0.05$ (b) $\eta = 0.1$ and structural properties stated in Figure 2.1.

For sound insulation purposes, a high damping is desirable, as the vibration would be much less.

The resonant bending wave field, however, depends on the loss factor. It is proportional to $10 \log(1/\eta)$ and to the total area of the structure [12, pp. 253]. To examine the damping in finite structures in real life, the structural reverberation time can be measured.

2.1.3 Structural Reverberation Time & Total Loss Factor

Analogous to the reverberation time of a room, the structural reverberation time T_s is defined as the time in seconds required for the level of velocity or acceleration in a structure to drop by 60 dB after the structure-borne sound source has stopped, as stated in section 3.8 in EN ISO standard 10848-1 [17]. It indicates how fast the vibrational energy dissipates, that a long reverberation time implies a slow energy decay and long-lasting vibration, while a short reverberation time shows a fast energy dissipation; and vice versa.

Barron [18] presented a revised theory of sound level distribution in rooms with a diffuse sound field and is illustrated in Figure 2.5.

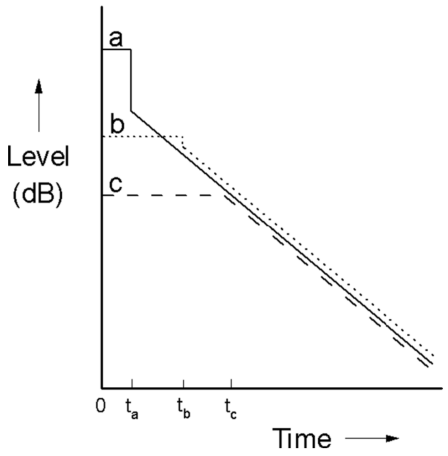

Figure 2.5: Theoretical integrated impulse curves at three receiver positions a, b, and c in a room with a diffuse sound field, extracted from [18].

In this model, the integrated impulse decays at three receiver positions are plotted in a common time scale, where $t = 0$ is when the sound is emitted from the source. Position a is the closest to the source with t_a the travel time for the direct sound. Position b is further away from the source and position a, and position c is the furthest among the three. It assumes that significant reflected energy is present after the arrival of the direct sound, with a linear decay. At any time $t > t_c$, the level decay curves overlap, i.e. the sound levels are the same at all three positions.

The assumption of a diffuse field is valid for frequencies higher than the Schroeder frequency in a room. For low frequencies, room modes and resonances are dominant and the revised theory needs to be modified. This applies the same to vibrational energy in structures. Therefore it is more appropriate to refer to it as reverberant field [13, pp. 167].

A 60 dB reduction corresponds to the energy decay by a factor of 10^{-6}, hence the relationship between the total loss factor η_{tot} and structural reverberation time can be described as

$$\eta_{\text{tot}} = \frac{6\ln(10)}{\omega T_s} \approx \frac{2.2}{fT_s}. \tag{2.17}$$

The total loss factor accounts for the wave energy conversion into heat across the structure (the internal loss factor), the transmission to other parts of the structure and radiation into air (the coupling loss factor CLF) [19, pp. 62].

For masonry-type structures, Craik [19, pp. 9, 67] provided an estimation of the total loss factor as a function of $\sqrt{f}$, as shown in Eq. 2.18 and illustrated in Figure 2.6 from 10 Hz to 1 kHz. The first term $f^{-1/2}$ is an approximation for the losses due to coupling, and the second term 0.015 is an approximation for the internal loss factor, i.e. losses due to conversion into heat. The corresponding structural

reverberation time is also presented.

$$\eta_{\text{tot}} \approx \frac{1}{\sqrt{f}} + 0.015. \tag{2.18}$$

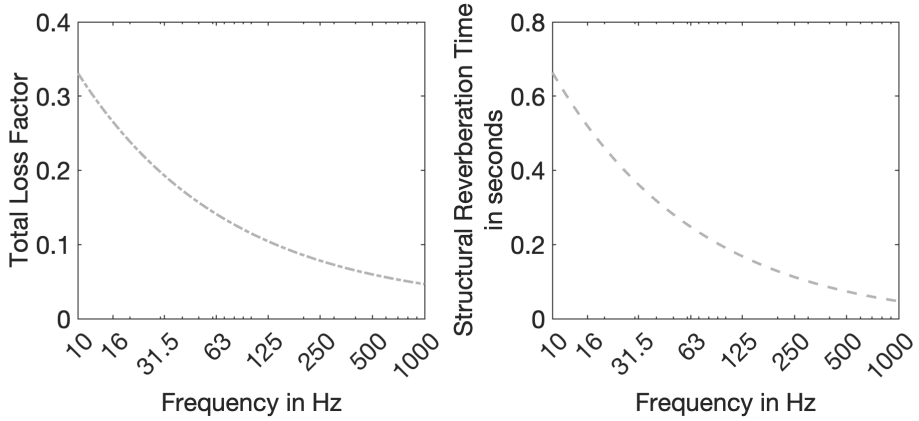

Figure 2.6: Estimation of η_{tot} as in Eq. 2.18 and corresponding T_s.

The estimated total loss factor for such structures is in the order of 10^{-1} and decreases with increasing frequency, which shows higher damping at lower frequencies. This may suggest a lower structural reverberation time at low frequencies. However, since the value is relatively small compared with frequency, the structural reverberation follows the same trend, that lower frequencies have a longer T_s, showing a slower energy dissipation and longer-lasting vibration.

The equation of the total loss factor due to the internal losses, the losses due to radiation and the losses at the perimeter of a structural element, an estimation for the laboratory situation and *in situ* can be found in EN ISO standard 12354-1 [20] in Formula (C.1), (C.3), (C.6) respectively.

2.1.4 Effective Speed

The integrated impulse curves as a function of time, $L(t)$, as shown in Figure 2.5, can be used to derive the level decay with time $\partial L/\partial t$ in (dB/s), which is the slope of the linear decay curve:

$$\frac{\partial L}{\partial t} = \frac{-60}{T_{60}}. \tag{2.19}$$

And the vibrational level as a function of distance, $L(r)$, can be used to derive the level decay with distance $\partial L/\partial r$ in (dB/m) by taking the derivative. Then the ratio of the two, the level decay as a function of time $\partial L/\partial t$ (dB/s) and that of distance $\partial L/\partial r$ (dB/m), equals an effective speed $\partial r/\partial t = c$ (m/s):

$$\frac{\partial L/\partial t}{\partial L/\partial r} = \frac{\partial r}{\partial t} = c. \tag{2.20}$$

If using T_d to represent the time for vibrational energy of the direct wave to decay 60 dB and replace it with η in Eq. 2.13, or in Eq. 2.15 with $N = 0$, and replace λ_B with c_B/f, the relative level becomes

$$\begin{aligned} L_B(r) &= -\frac{10\log_{10}(e)\pi}{c_B/f}\frac{6\ln(10)}{2\pi f T_d}r = -\frac{30}{c_B T_d}r; \\ \Rightarrow \frac{\partial L_B}{\partial r} &= -\frac{30}{c_B T_d}; \\ \Rightarrow \frac{\partial L/\partial t}{\partial L/\partial r} &= (-\frac{60}{T_d})/(-\frac{30}{c_B T_d}) = 2c_B = c_{gB}. \end{aligned} \tag{2.21}$$

The effective speed is found to be the group velocity in this case.

For $N = 10$ or 20, this effective speed is slower than the propagation phase speed c_B. Figure 2.7 shows the effective speed for an infinite structure with an estimated $\eta_{int} = 6 \cdot 10^{-3}$.

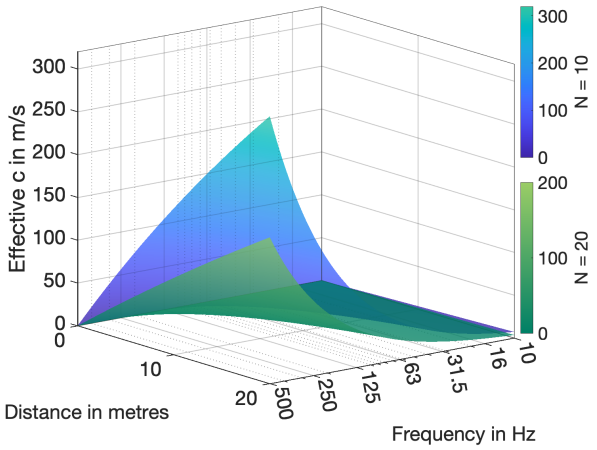

Figure 2.7: Estimation of the effective speed $\frac{\partial L/\partial t}{\partial L/\partial r}$ for $N = 10, 20$.

The effective speed varies with distance and frequency. It is greater at higher frequencies and longer distances. Similar analysis can be done for finite structures with measured vibration levels as a function of time and distance.

2.1.5 An Empirical Formula for Vibration Levels

Matsuda, Tachibana, and Ishii [21] proposed an empirical formula for vibration acceleration levels (V.A.L.) L_r based on field measurements and scale model experiments:

$$L_r = P_0 - N\log(r) - Mr, \tag{2.22}$$

where P_0 depends on the strength of excitation, N was found to be 20 from field measurements, and M in (dB/m) is determined in each octave band from measurements, and is approximately proportional to $\sqrt{f}$.

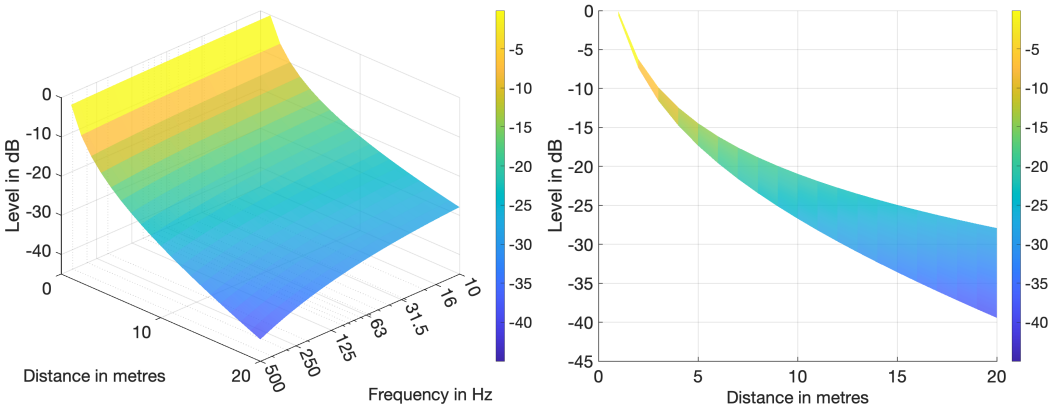

Figure 2.8: L_r in dB according to Eq. 2.22, with $P_0 = 0$, $N = 20$, and $M = 0.03\sqrt{f}$.

The empirical model gives similar results as in the previous sections, while the levels decay more substantially. The deviation can result from that the field measurements in [21] were carried out across rooms and storeys in buildings, and thus damping due to discontinuities of structures was included in addition to damping within structures.

2.2 Summary

To summarize, the propagation speed and relative vibration level of direct free bending waves in an infinite beam or plate can be estimated. The parameters needed to estimate vibration levels due to geometrical spreading and material damping are propagation speed c_B and an internal loss factor η_int. By re-writing Eq. 2.15, The relative vibration level at distance r is as follows:

$$\begin{aligned} L_\mathrm{B}(r) &= -N\log_{10}(r) - \frac{10}{\ln(10)}\frac{\pi\eta_\mathrm{int}r}{\lambda_\mathrm{B}} \\ &= -N\log_{10}(r) - \frac{10}{\ln(10)}\frac{\pi\eta_\mathrm{int}fr}{c_\mathrm{B}} \\ &= -N\log_{10}(r) - \frac{10}{\ln(10)}\frac{\omega\eta_\mathrm{int}r}{c_\mathrm{gB}}, \end{aligned} \tag{2.23}$$

with $N = 0$ for one-dimensional case (plane waves), $N = 10$ for two-dimensional case (cylindrical spreading) and $N = 20$ for three-dimensional case (spherical spreading). For the last two cases, this level follows a logarithmic decay due to the distance law. Low-frequency waves propagate slower with a much longer wavelength compared with that of higher frequencies, and thus decay considerably less.

For finite structures where both direct and reflected waves are present, the energy transportation can be seen from the effective speed (Eq. 2.20), which can be evaluated based on vibrational level decay as a function of time (dB/s) and distance (dB/m), requiring structural reverberation time evaluation. The total loss factor can be obtained through Eq. 2.17.

To evaluate the validity of the theories described above with such assumptions, vibration measurements were performed and presented in the following chapters (section 3 and 4).

3

Methods

As summarized in the previous section (2.2), the following parameters are under interest:

- propagation speed of waves with motion perpendicular to the surface
- vibration attenuation over distance
- structural reverberation time & the total loss factor.

Vibration measurements were performed on a concrete floor in a building. It took place on April 09, 2024, in the Gothenburg office of Brekke & Strand Akustik AB, located on the third floor at Södra Gubberogatan 4, 416 63, in Gothenburg, Sweden.

3.1 Measurement Setup

The structure under test was a 270-mm thick concrete floor. Figure 3.1 shows the floor plan of the office, with excitation and measurement positions marked.

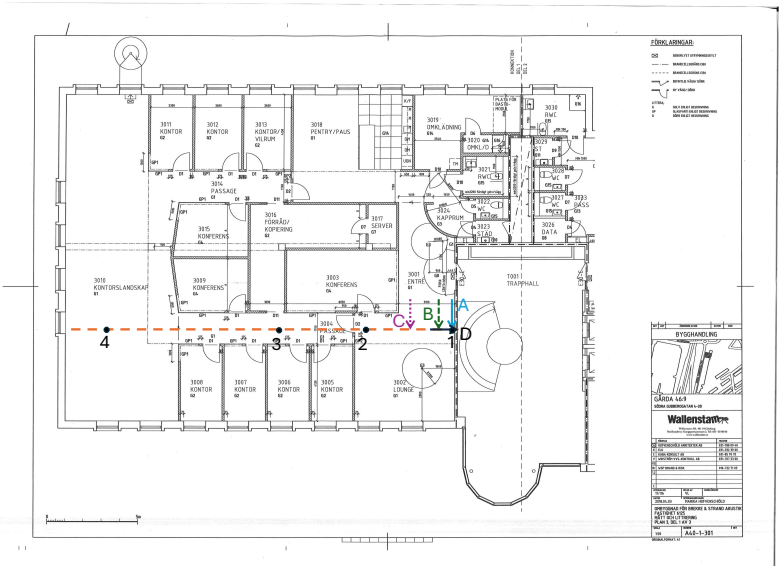

Figure 3.1: Floor plan of the office with marks of excitation positions A, B, C, D and measurement positions 1, 2, 3, 4.

According to the floor plan, the office floor can be roughly estimated as a rectangular plate with dimension 18.02 m × 25.21 m, measured from inner boundaries to the "KONNEKTION" (connection) between "Del 1" and "Del 2", ignoring the circular shape on the right corner. The floor is possibly assembled by two concrete plates, indicated by a connection of two dashed lines in the middle. The construction type of the concrete slab (solid, ribbed, hollow-core, etc.) is unknown.

The floor was hit by a 12-kg kettlebell at floor positions A, B, C, and on the wall position D, and the vibration accelerations normal to the floor surface at floor positions 1, 2, 3, and 4 were measured simultaneously with four ICP® accelerometers from PCB Piezotronics. The excitation and measurement positions were chosen so that the wave propagation along the positive x direction was measured. The distance was randomly chosen such that it spread out the surface. Data acquisition system SQuadriga III was used. See Appendix A.2 for a complete list of equipment. A schematic diagram of the setup is shown in Figure 3.2, and Figure 3.3 illustrates the excitation source and the measurement environment. The point excitations were on top of the carpet, and a rubber mat was used above it, acting as a low-pass filter. The vibrations were measured with accelerometers mounted directly onto the surface of the concrete floor.

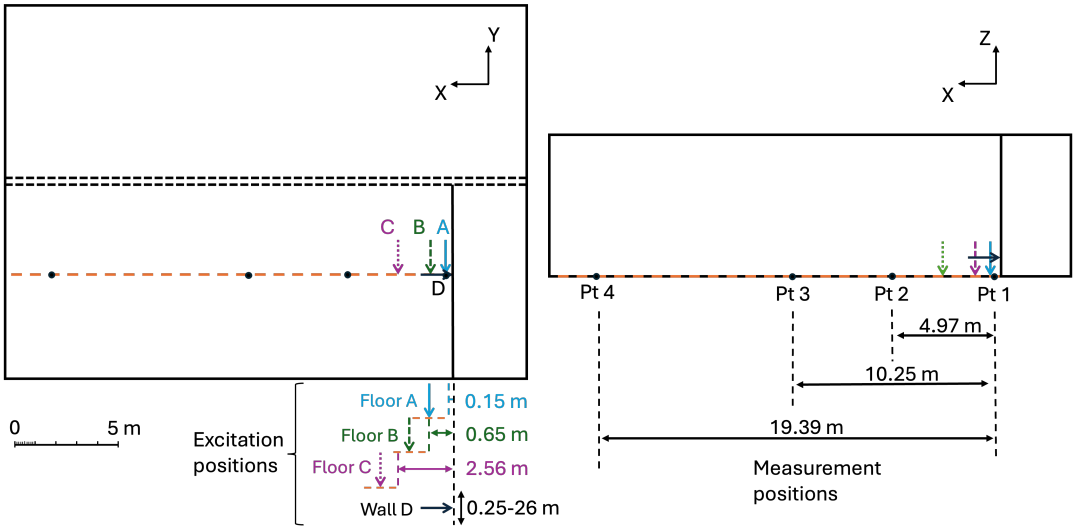

Figure 3.2: Schemetic diagram of the measurement setup.

For each point excitation, 8-10 hits of the dropped mass were manually applied with approximately the same strength to assess the repeatability and consistency of the results over a time period of 30 s to 40 s. A background noise measurement was done before excitations.

The boundary conditions are simply supported at the edges and clamped (or fixed) between the floor and the inner wall (indicated by a black solid line inside the plane. The wall is 190 mm thick with solid steel reinforced concrete, built from the entrance floor to the top floor of the building. Thus, the connection between the floor edge and the inner wall can be classified as a T junction. The excitation on the wall is

approximately 0.25 m to 0.26 m above the floor. This measurement was to test how discontinuities between structures would influence the results.

Measurement position Pt. 1 is near the junction of the floor and the inner wall, hence the motion is relatively small compared with that of Pt. 2, 3, and 4. Therefore this position was disregarded in the analysis of vibration levels for excitation positions B and C.

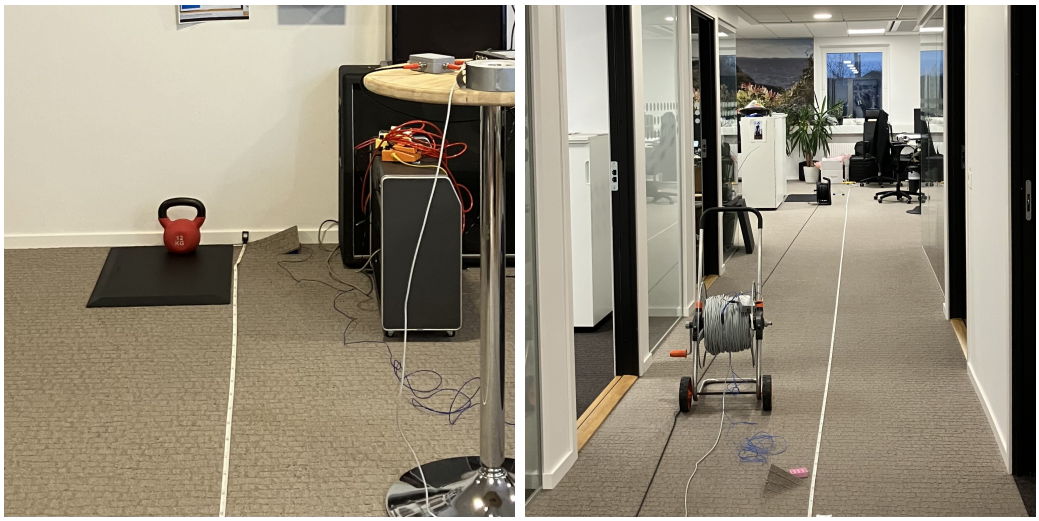

Figure 3.3: Photos of the excitation source (a 12-kg kettlebell) and the measurement environment.

3.2 Data Processing

The data was recorded with a sampling frequency of 48 kHz to ensure a precise representation of the captured signals. All measurement data were acquired through SQuadriga III and then processed in MATLAB.

A spectral analysis was performed for each measurement, where the autospectrum in terms of energy spectral density (ESD) [17, pp. 32] was computed with a block size of 2^{16} for the Fast Fourier Transform (FFT) and Hann window with an 50 % overlap. Thus the frequency resolution Δf was roughly 0.73 Hz. (See Figure 4.1.) The spectra in the 1/3-octave band were also computed (see Figure 4.2). The spectrograms for each impulse response are presented in Appendix B.1. In addition, the time signals were filtered using a filter bank created through `octaveFilterBank`[1] with 1/3 octave and a filter order of 10 in the frequency range from 10 Hz to 1000 Hz.

[1]MathWorks, Inc., "octaveFilterBank System object," MATLAB Documentation, 2024. Accessed: Oct. 30, 2024. [Online]. Available: `https://se.mathworks.com/help/audio/ref/octavefilterbank-system-object.html`

3.3 Propagation Speed

The propagation speed of waves (phase speed) with motions normal to the surface can be examined by the time delay between signals at different measurement positions, which was computed by the cross-correlation function. It was used to compute the direct wave propagation. For the entire signal with both direct and reverberant fields, the centre time was used.

3.3.1 Cross-Correlation Function

The cross-correlation function is a measure of the similarity of the signal $x(t)$ to $y(t)$ at a different time $y(t+\tau)$, where τ is the time delay [6, pp. 527], [22, pp. 60]. It is defined as

$$R_{xy}(\tau) = \int \mathrm{d}t \; x(t) \; y(t+\tau). \tag{3.1}$$

In MATLAB, this was achieved by using the built-in function `xcorr`[2].

3.3.2 Centre of Gravity

For analysis of the entire signal with both direct and reverberant fields, a propagation speed based on the centre of gravity of the energy was evaluated. The centre time t_s is the centre of gravity time [23] of the decaying vibration field, which is the time to reach half of the energy. It corresponds to the time to decrease by 3 dB from the initial energy level.

$$t_s = \frac{\int_0^\infty t \cdot a^2(t) dt}{\int_0^\infty a^2(t) dt}. \tag{3.2}$$

Figure 3.4 shows an example of the computation process. This is the first impulse response at Pt. 1, 2, 3, 4 with point excitation at position Floor A at 31.5 Hz center frequency band.

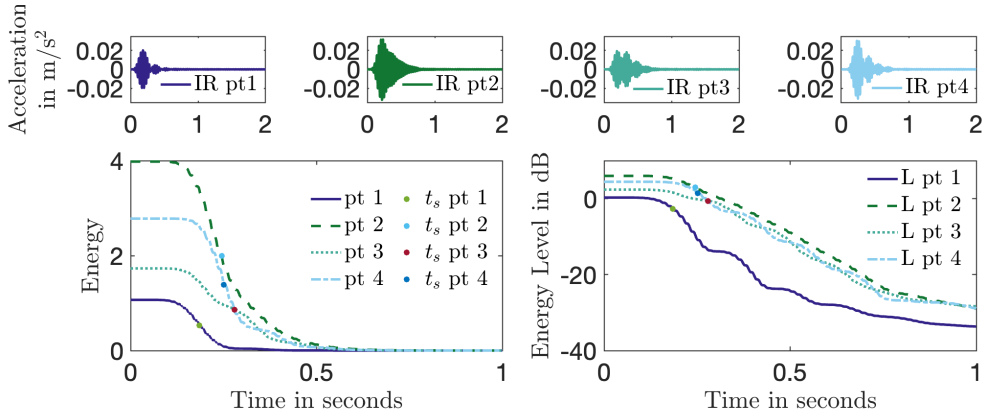

Figure 3.4: The impulse response and its energy from backward integration.

[2]MathWorks, Inc., "xcorr: Cross-correlation," MATLAB Documentation, 2024. Accessed: Oct. 30, 2024. [Online]. Available: `https://se.mathworks.com/help/matlab/ref/xcorr.html`

3.3.3 Computation Process

By computing the time delay in seconds between a reference measurement position and the rest at each frequency band as a function of distance in metres, and performing a linear fit to extract the slope in s/m, then taking the inverse, the propagation speed in m/s of waves at transverse motion can be obtained. For all excitation positions A, B, C, and D, the time delay was computed reference to Pt. 2 (compare 2-2, 2-3, 2-4); as for excitation positions Floor A and Wall D, the computation reference to Pt. 1 was also computed (compare 1-1, 1-2, 1-3, 1-4).

An example is shown in Figure 3.5, where the time delay of the acceleration at measurement positions reference to pt. 1 with excitation at position Floor A is computed for the filtered signals.

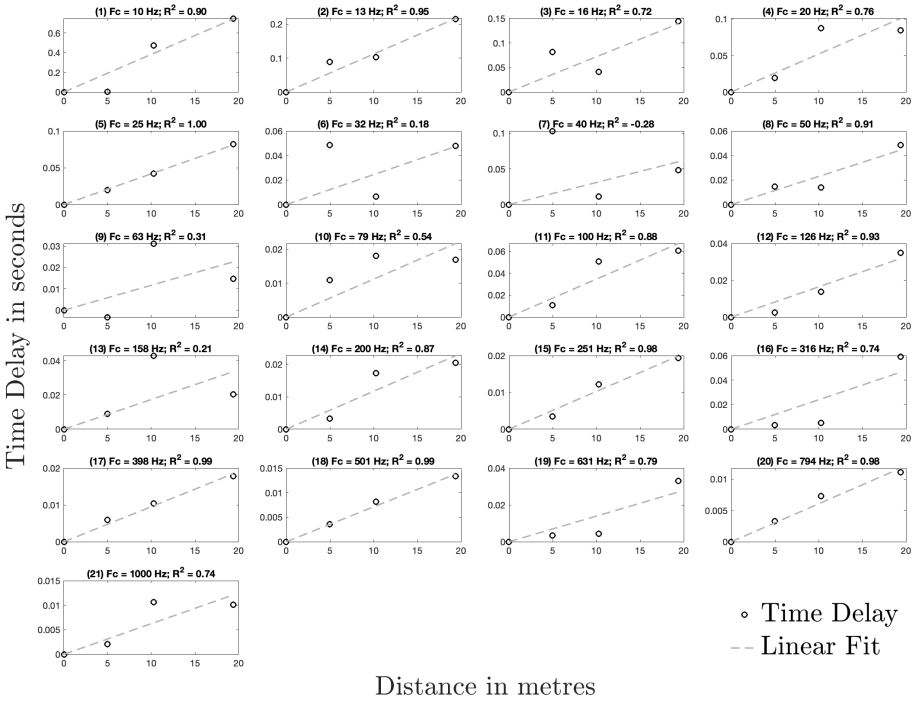

Figure 3.5: Time delay of the acceleration at measurement positions reference to Point 1, excited at position Floor A.

The fit was performed using the linear regression model `fitlm`[3] with x being the distances and responses y the time delay at the measurement positions, both reference to the reference point (pt.1 in this case). The `Intercept` was set to `false` to remove the constant term from the model. The coefficient of determination R^2 [24] was computed for each fit to see the validity of the model. The slope of the linear fit

[3]MathWorks, Inc., "fitlm: Fit linear regression model," MATLAB Documentation, 2024. Accessed: Oct. 30, 2024. [Online]. Available: `https://se.mathworks.com/help/stats/fitlm.html`

was then extracted for each frequency band and used to compute the propagation speed. A figure of the inverse of the slope as a function of center frequency bands was plotted and fit with $x = \sqrt{f}$, using `fitlm` and no intercept.

It is important to note that not all frequency bands were included in the fitting process. Specifically, the slopes of the time delay vs. distance fit with an R^2 value less than 0.7 were excluded to provide a more accurate representation of the propagation speed. The exclusion of these outliers is likely due to local anomalies or interference from boundary effects, which may include resonance with the eigenfrequencies (natural frequencies of structural vibrations) of the concrete floor, measurement noise, or the influence of reflected waves from the boundaries.

Figures of the time delay with the fit for each excitation position are presented in Appendix B.2 for reference. The results of propagation speeds are presented in the next chapter (section 4.2).

The computation for the centre time was based on the total energy computation, which was achieved by taking a backward integration of the square of acceleration value using `cumsum`[4]. Then, perform a linear fit on the centre time vs. distances plot as described for the time delay (similar to Figure 3.5). The propagation speed is the inverse of the slope of the fit.

3.4 Level Decay / Distance Attenuation

3.4.1 Direct Waves

The vibration level of direct waves was obtained by computing the acceleration level of the maximum amplitude of the acceleration at different positions, relative to the reference position. This assumes that the maximum amplitude is at the direct impulse, and no reflected waves have a higher amplitude than the direct wave.

$$L_r(i) = 10\log_{10}\left(\frac{\alpha^2_{\text{max, i}}}{\alpha^2_{\text{max, ref}}}\right) = 20\log_{10}\left(\frac{\alpha_{\text{max, i}}}{\alpha_{\text{max, ref}}}\right). \tag{3.3}$$

The predicted relative level was computed using Eq. 2.23 with obtained c_{B} and an estimated internal loss factor $\eta_{\text{int}} = 6 \cdot 10^{-3}$ for $N = 0, 10, 20$.

3.4.2 Entire Signal

The vibration level for the overall response was computed based on the total energy at the measurement position, which was achieved by the backward integration.

$$L_r(i) = 10\log_{10}(E_{\text{tot, i}}). \tag{3.4}$$

[4]MathWorks, Inc., "cumsum: Cumulative sum," MATLAB Documentation, 2024. Accessed: Oct. 30, 2024. [Online]. Available: `https://www.mathworks.com/help/matlab/ref/double.cumsum.html`

3.5 Structural Reverberation Time & Total Loss Factor

The loss factor η can be estimated based on the structural reverberation time for the vibration energy as described in Eq. 2.17, which is called the impulse response decay method [16]. The measurement and evaluation were conducted based on section 7.3 in EN ISO 10848-1 [17]. Excitation positions Floor A, B, C and measurement positions Pt. 2, 3, 4 were used for analysis. The decay curve of each impulse response was computed using a backward integration of the squared, filtered impulse response. Then the determination of T_{10}, T_{20}, T_{30} was evaluated by a linear fit performed from 5 dB to 15 dB, 25 dB, and 35 dB below the steady-state level. The coefficient of determination R^2 was evaluated for each fit and compared to decide the best value. With the slope of the best fit denoted as d, the relationship yields $T_s = 60/d$ for each impulse response. Finally, the structural reverberation time was determined by calculating the arithmetic averaging of the individual reverberation times.

Figure 3.6 shows an example of the computation process. This is the first impulse response at Pt. 3 with point excitation at position Floor A at 31.5 Hz center frequency band.

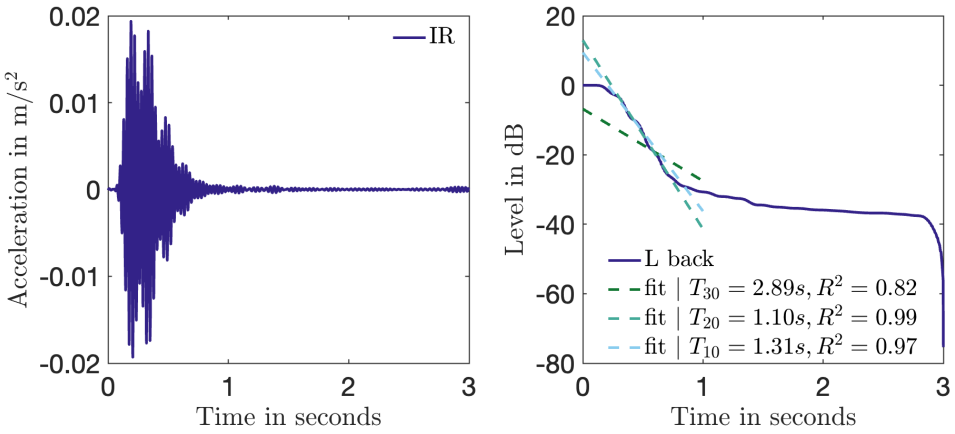

Figure 3.6: The impulse response and its level from backward integration. The decay curve fit calculated from T_{30}, T_{20}, and T_{10} was plotted from time period 0 to 1 s.

In this case, the decay curve of T_{20} gives the best R^2 value, and thus T_s is estimated using T_{20} for this impulse response.

The computation was repeated and automated to calculate the decay curve for each impulse response at the aforementioned excitation positions and measurement positions.

3.6 Effective Speed

The effective speed of waves was computed based on the ratio of dL/dt and dL/dr, as shown in Eq. 2.20. The first term was evaluated from the structural reverberation time as in Eq. 2.19, and the second term was evaluated based on the derivative of the level decay curve as a function of distance. The derivative was computed using the difference of the vibration level between measurement positions using `diff`[5]:

$$\frac{\partial L}{\partial r} = \frac{\mathrm{diff}(L)}{\mathrm{diff}(r)}. \tag{3.5}$$

Compute these values for each frequency band. Then take the ratio of the two to obtain the effective speed as a function of frequency.

[5]MathWorks, Inc., "diff: Differences and approximate derivatives," MATLAB Documentation, 2024. Accessed: Oct. 30, 2024. [Online]. Available: `https://www.mathworks.com/help/matlab/ref/double.diff.html`

4

Results

The vibration measurement results regarding propagation speed, structural reverberation time, total loss factor, and distance attenuation were computed based on section 3 and presented as follows.

4.1 Frequency Spectra

Figure 4.1 shows the autospectrum of the acceleration value at each measurement position for each excitation. The computation was specified in section 3.2. The autospectra in one-third octave bands is shown in Figure 4.2. Several peaks observed in the background noise at 12.5 Hz, 19 Hz, 60 Hz are possibly due to building vibrations and/or mechanical equipment such as HVAC systems; and distinctive peaks at 50 Hz, 100 Hz, 150 Hz and 200 Hz are likely to be the electrical noise and its harmonics.

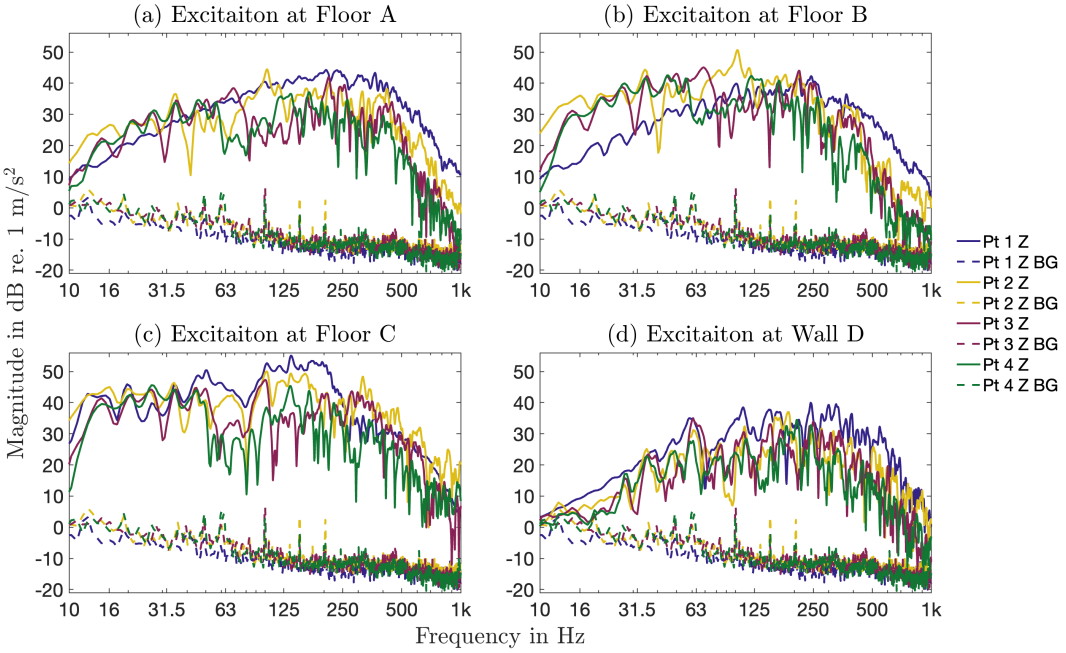

Figure 4.1: Autospectra of acceleration at each measurement position, excited at position (a) Floor A, (b) Floor B, (c) Floor C, and (d) Wall D.

As explained in section 3.1, due to the proximity between pt. 1 and the fixed boundary, the modes at low frequencies were more difficult to excite, which can be seen from Figure 4.1 and Figure 4.2 (a) below 160 Hz, and (b) below 250 Hz, where excitation is close to pt. 1. For frequency bands higher than that the magnitude follows pt.1 > pt.2 > pt. 3 > pt.4 in general, and this trend holds for (d) at all frequency bands. When excitation was at (c) Floor C, where pt. 2 is relatively close, it had more energy than that of the other three positions, except in the frequency bands between 31.5 Hz and 150 Hz, where pt. 1 had the most energy. The floor was mostly excited in the bands between 63 Hz and 500 Hz for all excitations.

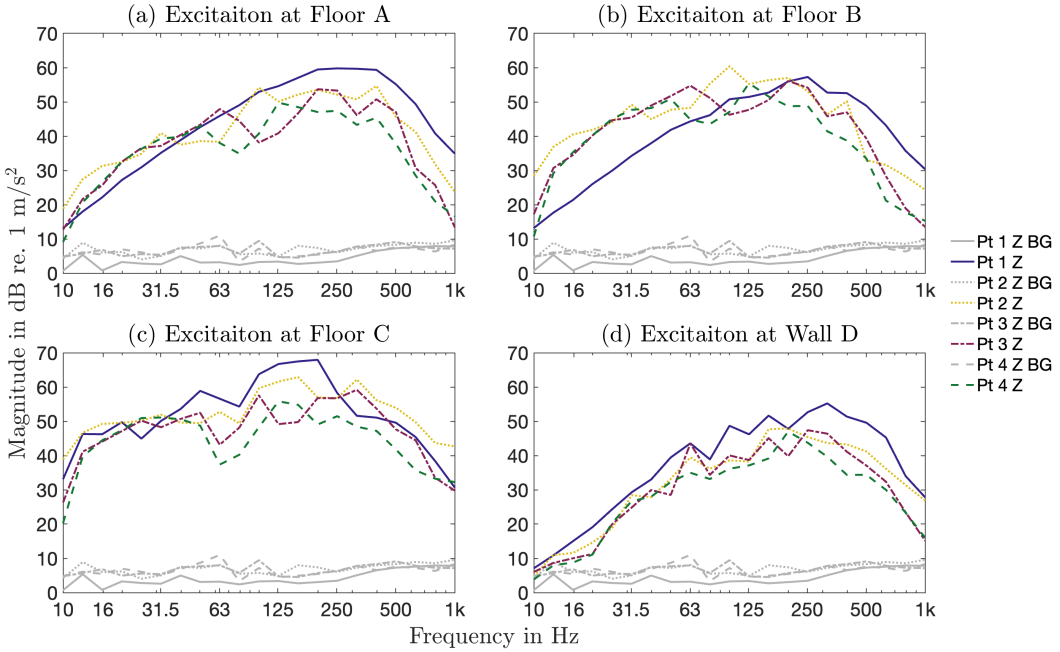

Figure 4.2: Autospectra of acceleration at each measurement position in one-third octave bands, excited at position (a) Floor A, (b) Floor B, (c) Floor C, and (d) Wall D.

4.2 Time Delay & Propagation Speed

The time delay and propagation speed for unfiltered and filtered signals are presented as follows.

4.2.1 Unfiltered Signals

The time delay of unfiltered signals was computed as described in section 3.3, shown in Figure 4.3, and the corresponding propagation speed based on the slope of the fit is shown in Table 4.1.

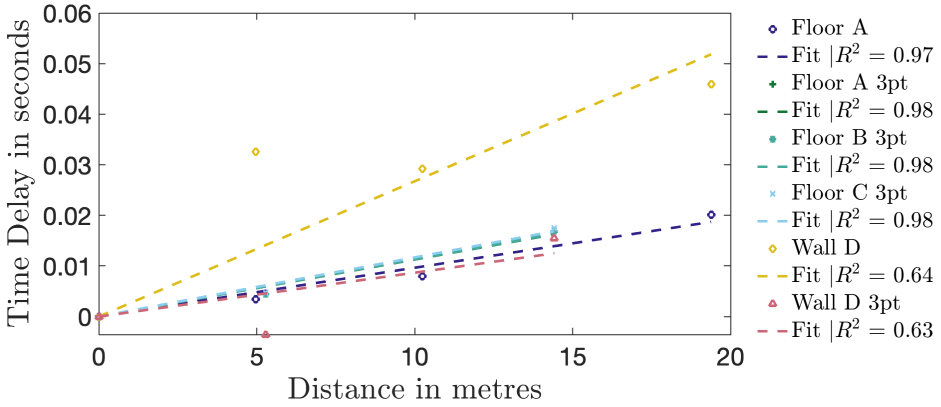

Figure 4.3: Time delay of the acceleration at measurement positions reference to a reference point at each excitation position.

Excitation Pt.	Floor A	Floor B	Floor C	Wall D
Propagation Speed ref. pt. 1	1036	/	/	374
Propagation Speed ref. pt. 2	887	883	855	1153

Table 4.1: Propagation Speed of Unfiltered Signals.

For the propagation speed of unfiltered signal based on the linear fit of time delays between measurement positions, an average speed of approximately 875 m/s was found for excitation on the floor with reference to pt. 2. This value is in close agreement with the results reported in [5] (833 m/s), with a 5 % difference. A faster propagation speed was observed for excitation on Floor A with reference to pt. 1 (1036 m/s).

When the floor is excited by the wall, the propagation speed of the unfiltered signals was slower (374 m/s) with reference to pt. 1, but faster (1153 m/s) with reference to pt. 2. These variations suggest that further measurements are necessary to conduct a more comprehensive and versatile comparison of propagation speeds across different excitation positions and conditions.

4.2.2 Filtered Signals

The same analysis was performed on the filtered signals, with figures of time delay shown in Appendix B.2 and propagation speed as a function of frequency presented in Figure 4.4. The corresponding Young's modulus was calculated based on equations in Table 2.1 and presented in Table 4.2. Equations for both beams and plates were used.

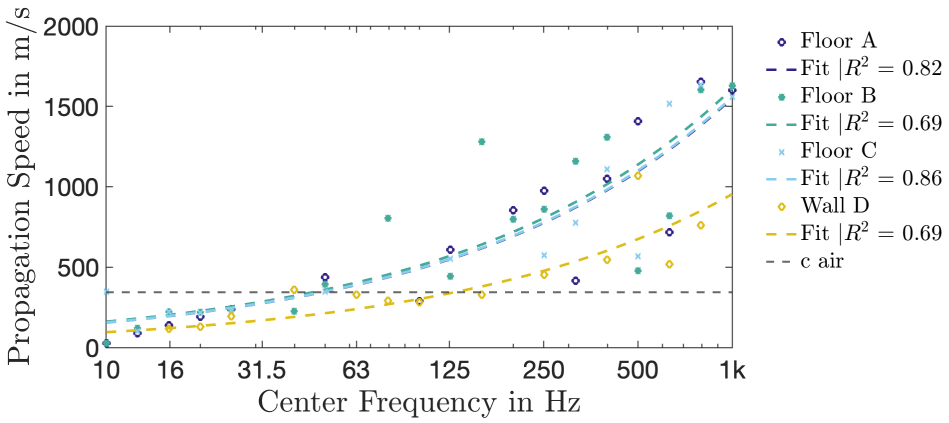

Figure 4.4: Propagation speed of the acceleration at measurement positions.

The propagation speed of wave motion normal to the floor surface generally follows the speed of bending waves ($c_B \propto \sqrt{f}$), and a slower speed was found for excitation on the wall compared with those on the floor. The critical frequency was found to be approximately 50 Hz for excitations on the floor and 125 Hz for excitations on the wall.

Excitation Pt.	Floor A	Floor B	Floor C	Wall D
E_{beam} in GPa	57.9	67.1	58.8	8.28 | 16.7
E_{plate} in GPa	55.6	64.5	56.4	7.95 | 16.1

Table 4.2: Young's Modulus based on the fit of c_B. For excitation Wall D, values based on the thickness of the floor (270 mm) and the wall (190 mm) were both calculated, where the left number is based on the thickness of the floor and the right is based on the wall.

The Young's modulus calculated using equations for beams and plates has an average value of 61.3 GPa and 58.8 GPa respectively, when the excitation positions were on the floor, assuming a density of 2400 kg/m^3 for concrete. This value is larger than the typical range of 14-41 GPa [10], which may suggest that a stiffer material is present within the structure, such as high-strength aggregates, additional reinforcement, or specific additives that enhance the material's stiffness.

In contrast, a lower propagation speed was observed for excitation on the wall, and the modulus of elasticity was significantly lower than that on the floors, falling outside the typical range if the calculation was based on the thickness of the floor. The values calculated based on the thickness of the wall are more reasonable. This discrepancy may result from the differences in the material properties of the wall - the wall is thinner (190 mm-thick) - the interaction between the wall and the floor, or potential measurement artifacts. Further measurements and analysis are required to fully understand the causes of this variation.

4.3 Level Decay / Distance Attenuation

With obtained c_B from measurement and an estimated η_{int} of $6 \cdot 10^{-3}$, the expected vibration levels of direct waves were predicted using Eq. 2.23 and shown in Figure 4.5. The c_B used here is from the fit of Floor A shown in Figure 4.4. The relative vibration acceleration levels for all three cases, one-dimensional ($N = 0$), two-dimensional ($N = 10$), and three-dimensional ($N = 20$), were all plotted. Then it is compared with measurements at different excitations shown in Figure 4.6, 4.7, 4.8, and 4.9.

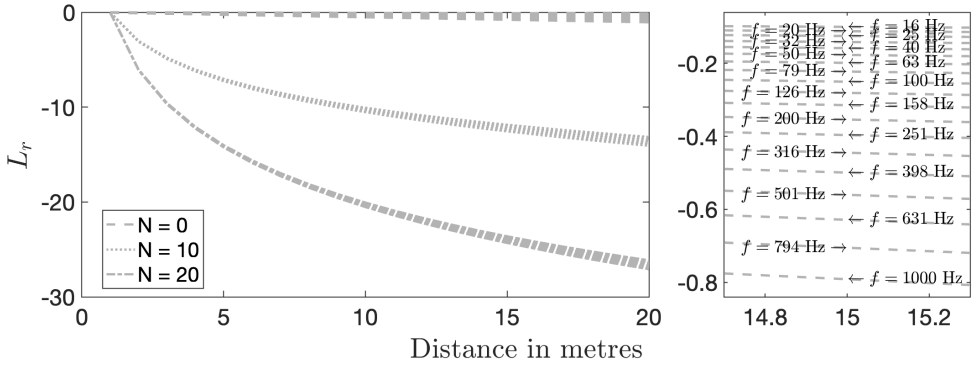

Figure 4.5: Vibration level predicted using Eq. 2.23, with c_B found in the fit of propagation speed excited at position Floor A (see Figure 4.4) and an estimated $\eta_{int} = 6 \cdot 10^{-3}$.

As can be seen in Figure 4.5, the vibration level at 16 Hz frequency band decays the least compared with those at higher frequencies, and the level at 1000 Hz decays the most.

Figure 4.6 shows the measured relative acceleration level as a function of distance, reference to pt. 2, excited at position Floor A.

From Figure 4.6, distinct patterns can be observed below and above 70 Hz. The vibration acceleration level for frequencies below 70 Hz follows the plane wave propagation ($N = 0$), while for frequencies above 70 Hz, it spreads cylindrically ($N = 10$). This behaviour may be due to the fact that the width of the plate is relatively small compared to the wavelength of the bending wave, causing it to behave like a beam, with low-frequency waves travelling primarily in the x direction. The width of the plate is approximately 9 metres, which is roughly twice the wavelength of the bending wave at 70 Hz in this scenario.

Theoretically, the vibrational level of the direct wave should decay as it propagates, either due to internal material losses or geometrical spreading. However, the measurement data occasionally show an increase in level with distance, suggesting that the wave does not lose energy as it propagates. This unusual behaviour may be attributed to resonance effects or standing waves caused by reflections, where constructive interference occurs and amplifies the signal at specific distances. It is also

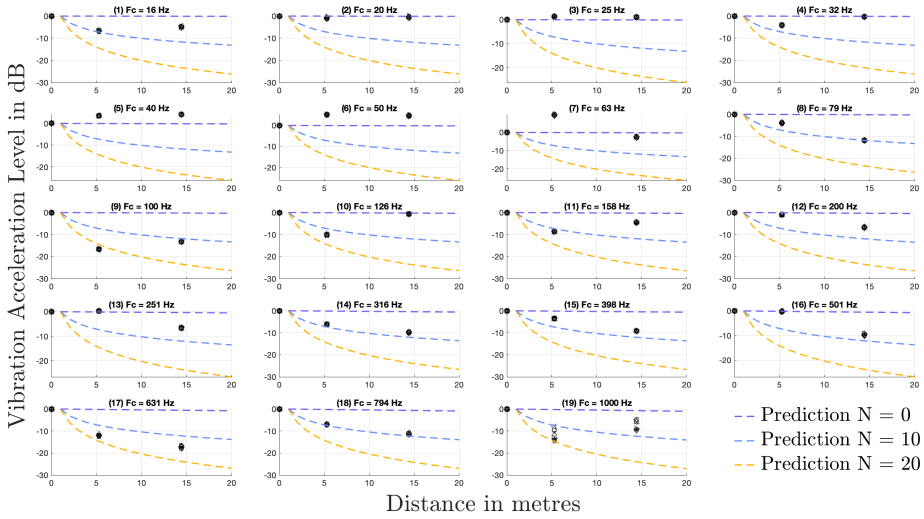

Figure 4.6: Vibration acceleration level at measurement positions reference to pt. 2, excited at position Floor A.

worth noting that the excitation position (Floor A) is close to the clamped boundary, which reduces vibrations near the boundary.

Similarly, Figure 4.7 shows the measured relative acceleration level with reference to pt. 2, excited at position Floor B, and Figure 4.8 shows the results for excitation at Floor C. The propagation speed used here is adapted to the corresponding fit found in Figure 4.4 for each curve.

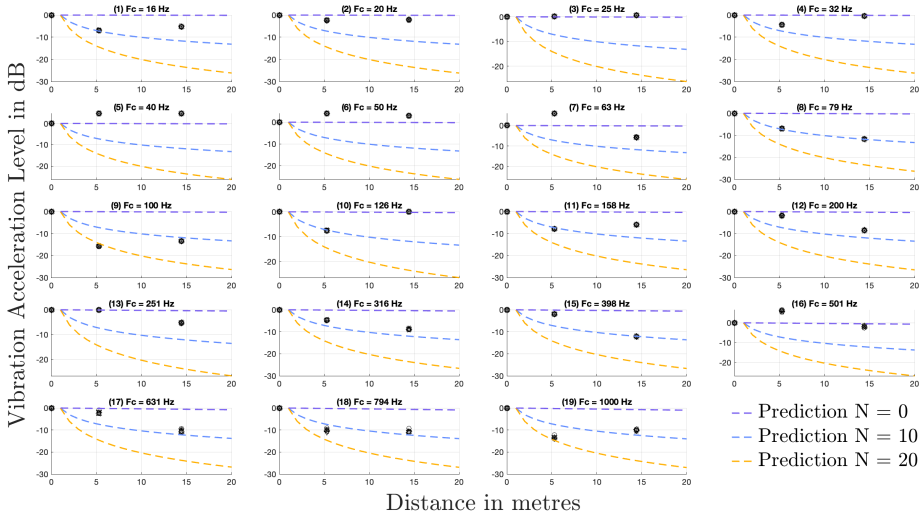

Figure 4.7: Vibration acceleration level at measurement positions reference to pt. 2, excited at position Floor B.

A similar pattern can be observed in both figures: at low frequencies ($< 60\,\mathrm{Hz}$ or

70 Hz), little decay is observed; while at higher frequencies, the wave exhibits cylindrical propagation. As the frequency increases, the level decays more significantly.

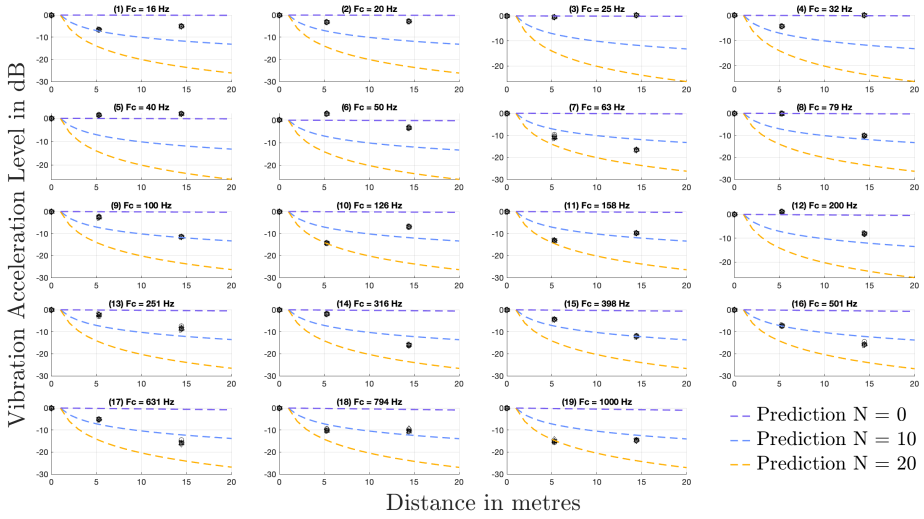

Figure 4.8: Vibration acceleration level at measurement positions reference to pt. 2, excited at position Floor C.

This suggests that, for direct waves, the wave follows plane wave propagation without geometrical losses when the width of the structure is smaller than two wavelengths. Frequencies above this threshold follow logarithmic decay, with geometrical spreading becoming dominant. Larger rates of decay with distance are observed as the frequency increases. However, additional measurements with more measurement points at various distances are needed to confirm this hypothesis.

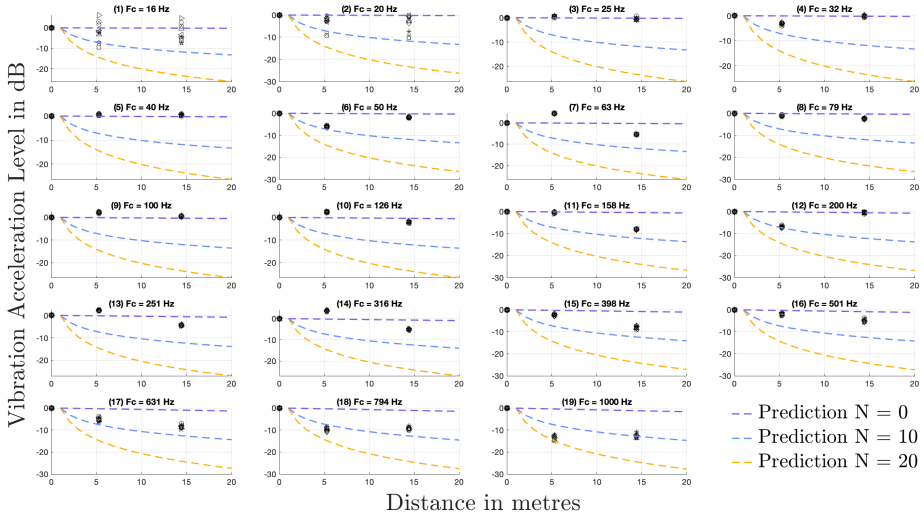

Figure 4.9: Vibration acceleration level at measurement positions reference to pt. 2, excited at position Wall D.

Figure 4.9 presents the case where the excitation was applied to the wall, with pt. 2 as the reference point. In this case, the vibrational level decay mostly follows one-dimensional plane wave propagation, with more decay occurring in the higher frequency range. When pt. 1 is used as the reference point, as shown in Figure 4.10, the majority of the measurement data align with the two-dimensional decay model.

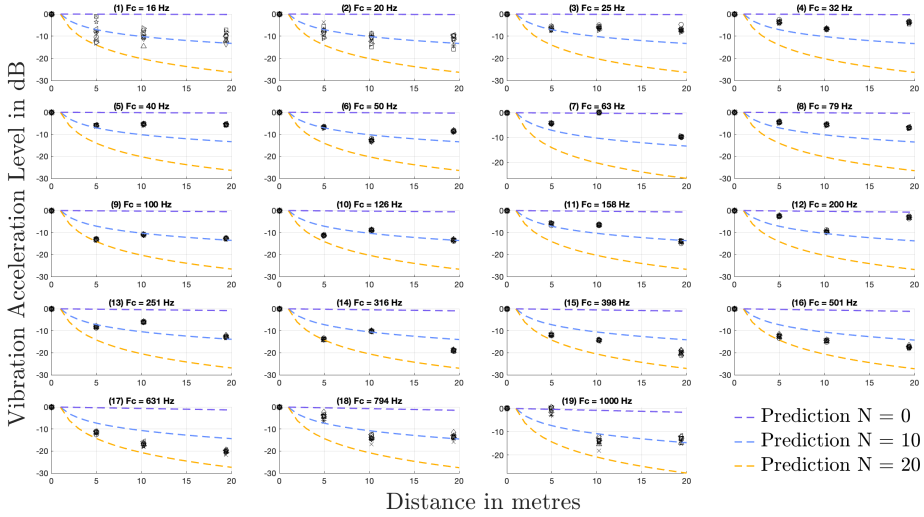

Figure 4.10: Vibration acceleration level at measurement positions reference to pt. 1, excited at position Wall D.

The difference in decay patterns between excitation on the floors and the wall can likely be attributed to the damping effects caused by the structural discontinuity between the floor and the wall, which can result in greater energy loss. Further measurements are required to conclude.

The results presented here correspond to the direct wave propagation. The following sections will present the analysis of waves that include both direct and reflected components.

4.4 Structural Reverberation Time & Total Loss Factor

The structural reverberation time T_s and the corresponding total loss factor η_{tot} calculated according to Eq. 2.17 in the centre frequency band between 16 Hz to 1 kHz, are shown in Figure 4.11. The signal-to-noise ratio was too low (less than 25 dB) to obtain a clear decay curve outside this frequency range, as shown in Figure 4.2.

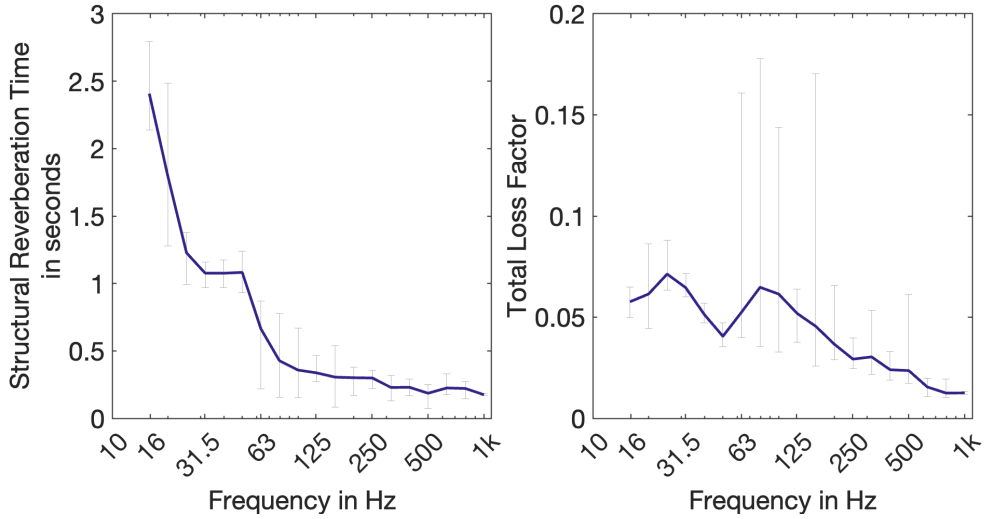

Figure 4.11: Measurement results of averaged T_s and corresponding η_{tot} calculated according to Eq. 2.17.

As expected, the structural reverberation time decreases with increasing frequency, ranging from 2.41 s at the lowest frequency (16 Hz) to 0.18 s at higher frequencies. It follows the same trend as in Figure 2.6, where T_s is higher at lower frequency, indicating slower energy dissipation and longer-lasting vibration. T_s is lower than 0.5 for frequencies higher than 63 Hz.

The structural reverberation time in the frequency band between 31.5 Hz and 50 Hz was found to be nearly constant (approximately 1.08 s), and a local minimum of 0.04 at 50 Hz is observed in the total loss factor plot. This coincides with the critical frequency found in Figure 4.4. Other than that, the total loss factor generally follows a similar decaying pattern as seen in Figure 2.6, with a decrease in the total loss factor as frequency increases. It ranges from 0.071 to 0.013.

As explained in the section 2.1.3 (Theory part), the total loss factor includes both internal material loss and the coupling loss factor. Assuming the internal loss remains constant, a decrease in the total loss factor at 50 Hz suggests a reduction in the coupling loss factor, i.e. the loss due to structural discontinuities (connections) or sound radiation is small at this frequency.

4.5 Effective Speed

The effective speed was computed using Eq. 2.20. Figure 4.12 shows an example when the floor is excited at Floor C. Generally, the effective speed is found to be lower than the propagation speed, indicating slower energy propagation. However, additional measurement positions are needed for the analysis to draw a conclusion.

It should be noted that the calculation for dL/dr is averaged over the distance due to the limited number of measurement points. Negative effective speeds are observed in the figure, which results from a positive level decay over distance. This

may be attributed to local anomalies or interference from boundary effects, which could include resonance with the eigenfrequencies (natural frequencies of structural vibrations) of the concrete floor, measurement noise, or the influence of reflected waves from the boundaries.

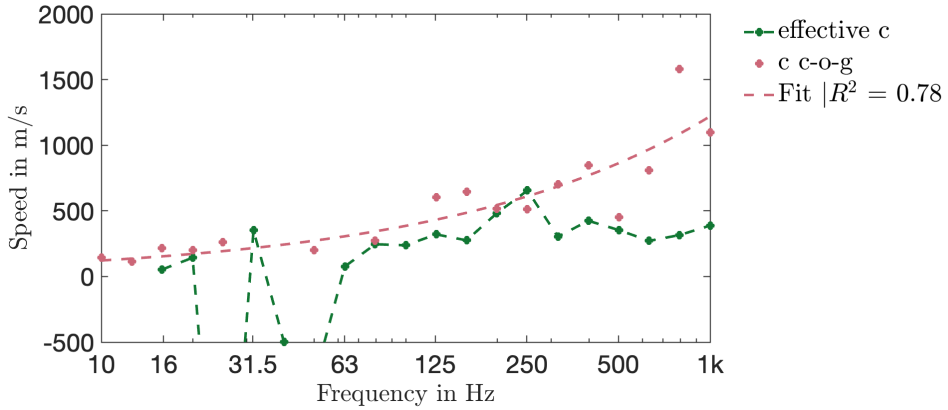

Figure 4.12: Effective speed based on the ratio of $(dL/dt)/(dL/dr)$, compared with the propagation speed computed from the centre time (centre of gravity time). Excited at position Floor C.

5

Conclusion

This thesis aims to understand the following questions, as outlined in section 1.3:

- Test the model and hypothesis presented in Østvik's report.
  - Is there a significant relationship between the temporal decay and the attenuation over distance for velocities in a building structure, measured within the same octave band?
    - Can this relationship be predicted?
    - Is it related to the propagation speed of waves in structures?

As discussed in section 2, the distance attenuation of direct wave vibration levels in a plate can be predicted by calculating the relative vibration level at distance r. The proposed equation, as shown in Eq. 2.23, links this attenuation to the propagation speed c_B of bending waves (waves with motion normal to the structural surface) and the loss factor η of the structure.

An empirical approach was used to validate this relationship through vibration measurements conducted on a concrete floor within an office building. Multiple excitation positions on the floor and wall were used to assess the propagation speed by analyzing the time delays of signals at various distances.

5.1 Key Findings

- **Propagation Speed** - Results show that the propagation speed of bending waves is proportional to the square root of frequency, as expected. Waves at low frequencies propagate much slower with longer wavelengths. A lower speed was observed when the floor was excited indirectly on the wall compared to direct excitation on the floor, which may be due to the smaller thickness of the wall.
- **Level Decay / Distance Attenuation** - For direct waves, the level decay with distance can be predicted using the obtained propagation speed c_B. The predicted level decay, accounting for internal material loss and geometrical spreading, was compared with measured data. It was observed that the

level decay follows plane wave propagation when the width of the structure is smaller than twice the wavelength of the bending waves. Frequencies above this threshold follow logarithmic decay due to geometrical spreading, with larger rates of decay observed as frequency increases.

- **Structural Reverberation Time & Total Loss Factor** - The total loss factor η_{tot} was determined using the impulse response decay method, which involved measuring the structural reverberation time T_s. T_s was found to decrease with increasing frequency, indicating a longer-lasting vibration at lower frequencies. A greater value of η_{tot} was found at lower frequencies, suggesting greater energy dissipation per oscillation at low frequencies.
- **Effective Speed** - The proposed effective speed, defined as the ratio of the vibrational level decay with time to level decay with distance (see Eq. 2.20), was theoretically found to equal the group speed of bending waves, in the case of an infinite beam (1D) with only material damping (internal loss) (see Eq. 2.21). It was computed and compared with the propagation speed of waves in structures from measurements. The effective speed was observed to be lower than the propagation speed, though further measurements are needed to explore the relationship between the two.

In conclusion, the level decay of direct waves with motion perpendicular to the structural surface can be estimated using the propagation speed of bending waves and the internal loss factor of the structure. The results provide valuable insights into understanding low-frequency structure-borne sound in concrete structures. Further measurements, including additional excitation and measurement positions at various distances, are required to validate the proposed relationships and explore the variations observed in this study.

5.2 Limitations and Future Work

Due to several constraints, the analysis in this thesis was limited to a single concrete floor. Future studies could address the following aspects:

- **Excitation source** - A kettlebell was used due to limited equipment availability. An electrodynamic shaker or impact hammer is preferred for better control over the input and improved signal-to-noise ratio (SNR).
- **Measurement positions** - Vibration was measured at four positions in one direction in this study. More measurement points and different directions should be considered in future analyses. Additionally, measurements across multiple rooms in a building should be taken to account for attenuation due to structural discontinuities/connections.
- **Level decay prediction** - The theory assumes that bending waves propagate in one direction. Future work could include equations that account for both x and y directions for level decay prediction. The prediction for level decay over

distance could also consider both direct and reverberant fields; measurement data can be compared with the empirical method based on Eq. 2.22 from [21].

- **Numerical models** - Finite element analysis (FEA) could be considered to simulate the structure. Some proposed methods provide foundations for predicting low-frequency structure-borne sound in concrete structures during the design stage, such as the finite-difference time-domain method (FDTD) by Asakura et al. [16], which focuses on a wall-type construction, and a hybrid FEM-SEA model developed by Sadeghi and Vasheghani [4], investigating structure-borne noise (SBN) induced by metro.

Bibliography

[1] B. Berglund, P. Hassmén, and R. F. S. Job, "Sources and effects of low-frequency noise," *The Journal of the Acoustical Society of America*, vol. 99, no. 5, pp. 2985–3002, May 1996, doi: 10.1121/1.414863. 1

[2] G. Leventhall, "Low Frequency Noise. What we know, what we do not know, and what we would like to know," *Journal of Low Frequency Noise, Vibration and Active Control*, vol. 28, no. 2, pp. 79–104, Jun. 2009, doi: 10.1260/0263-0923.28.2.79. 1

[3] T. Gjestland, "Low frequency sound insulation in building," SINTEF, Trondheim, Norway, SINTEF A210, June 22, 2006. Accessed: Mar. 05, 2024. [Online]. Available: https://sintef.brage.unit.no/sintef-xmlui/handle/11250/2387703 1

[4] J. Sadeghi and M. Vasheghani, "Improvement of current codes in design of concrete frame buildings: Incorporating train-induced structure borne noise," *Journal of Building Engineering*, vol. 58, p. 104955, Oct. 2022, doi: 10.1016/j.jobe.2022.104955. 1, 35

[5] L. Østvik, "Utbredelse av strukturlyd i større bygninger i betong. En måleoppgave.," NTNU, Trondheim, Trøndelag, Norway, Rep. Dec. 2018. 1, 2, 25

[6] T. D. Rossing, "Introduction to Acoustics," in *Springer Handbook of Acoustics*, T. D. Rossing, Ed., New York, NY: Springer, 2014. doi: 10.1007/978-1-4939-0755-7_1. 1, 18

[7] L. Cremer, M. Heckl, and B. A. T. Petersson, *Structure-Borne Sound*. Berlin, Heidelberg: Springer, 2005. doi: 10.1007/b137728. 1, 3, 4, 5, 6

[8] Frank Fahy and Paolo Gardonio, *Sound and Structural Vibration: Radiation, Transmission and Response*, vol. 2nd ed. Amsterdam: Academic Press, 2007. 1, 3, 5

[9] *Acoustics – Laboratory measurement of sound insulation of building elements – Part 4: Measurement procedures and requirements (ISO 10140-4:2021)*, Ref. No. EN ISO 10140-4:2021: E, European Standard, Apr. 2021. 1

[10] "Concrete Properties." Accessed: Oct. 30, 2024. [Online]. Available: https:

//www.engineeringtoolbox.com/concrete-properties-d_1223.html 5, 26

[11] *Building acoustics – Estimation of acoustic performance of buildings from the performance of elements – Part 2: Impact sound insulation between rooms (ISO 12354-2:2017)*, Ref. No. EN ISO 12354-2:2017 E, European Standard, Apr. 2017. 6

[12] M. Kleiner, *Acoustics and Audio Technology*. U.S.A.: J. Ross Publishing, 2012. 7, 9

[13] C. Hopkins, *Sound insulation*, 1st ed. Amsterdam: Elsevier / Butterworth-Heinemann, 2007. Available: https://www.arauacustica.com/files/noticias/pdf_esp_1296.pdf 7, 10

[14] N. Rawlinson. (2007). PEAT8002 - SEISMOLOGY Lecture 5: Surface waves and dispersion [PowerPoint slides]. Available: https://rses.anu.edu.au/~nick/teachdoc/lecture5.pdf 7

[15] N. Vardaxis. (2021). VTAF 01 – Sound in Buildings and Environment 6. Sound propagation [PowerPoint slides]. Available: https://www.akustik.lth.se/fileadmin/tekniskakustik/education/2021_VTAF01/NV6_SoundProp_23Apr2021_VTAF01.pdf 7

[16] T. Asakura, T. Ishizuka, T. Miyajima, M. Toyoda, and S. Sakamoto, "Prediction of low-frequency structure-borne sound in concrete structures using the finite-difference time-domain method," *The Journal of the Acoustical Society of America*, vol. 136, no. 3, pp. 1085–1100, Sep. 2014, doi: 10.1121/1.4892784. 21, 35

[17] *Acoustics – Laboratory and field measurement of flanking transmission for airborne, impact and building service equipment sound between adjoining rooms – Part 1: Frame document (ISO 10848-1:2017)*, Ref. No. EN ISO 10848-1:2017 E, European Standard, Oct. 2017. 9, 17, 21

[18] M. Barron, "Theory and measurement of early, late and total sound levels in rooms," *The Journal of the Acoustical Society of America*, vol. 137, no. 6, pp. 3087–3098, Jun. 2015, doi: 10.1121/1.4919655. xvii, 10

[19] R. J. M. Craik, *Sound Transmission Through Buildings: Using Statistical Energy Analysis*. England: Gower Publishing Limited, 1996. 10

[20] *Building acoustics – Estimation of acoustic performance of buildings from the performance of elements – Part 1: Airborne sound insulation between rooms (ISO 12354-1:2017)*, Ref. No. EN ISO 12354-1:2017 E, European Standard, Apr. 2017. 11

[21] Y. Matsuda, H. Tachibana, and K. Ishii, "Propagation Characteristics of Solid-Borne Sound in Building Structures," *The Journal of the Acoustical Society of Japan*, vol. 35, no. 11, pp. 609–615, 1979, doi: 10.20697/jasj.35.11_609. 12, 13, 35

[22] István L. Vér and Leo L. Beranek, Eds., *Noise and Vibration Control Engineering: Principles and Applications*, 2nd. ed. Hoboken, New Jersey: John Wiley Sons, Inc., 2006, doi: 10.1002/9780470172568. 18

[23] Octávio Inácio, "Fundamentals of Room Acoustics," presented at the IACMA - International Advanced Course on Musical Acoustics, Bologna, Italy, Jul. 2005. [Online]. Available: https://www.arauacustica.com/files/publicaciones_relacionados/pdf_esp_175.pdf 18

[24] Newcastle University, "Coefficient of Determination (R-squared)," Newcastle University. Accessed: Oct. 30, 2024. [Online]. Available: https://www.ncl.ac.uk/webtemplate/ask-assets/external/maths-resources/statistics/regression-and-correlation/coefficient-of-determination-r-squared.html 19

A

Appendix 1

A.1 Floor Plan

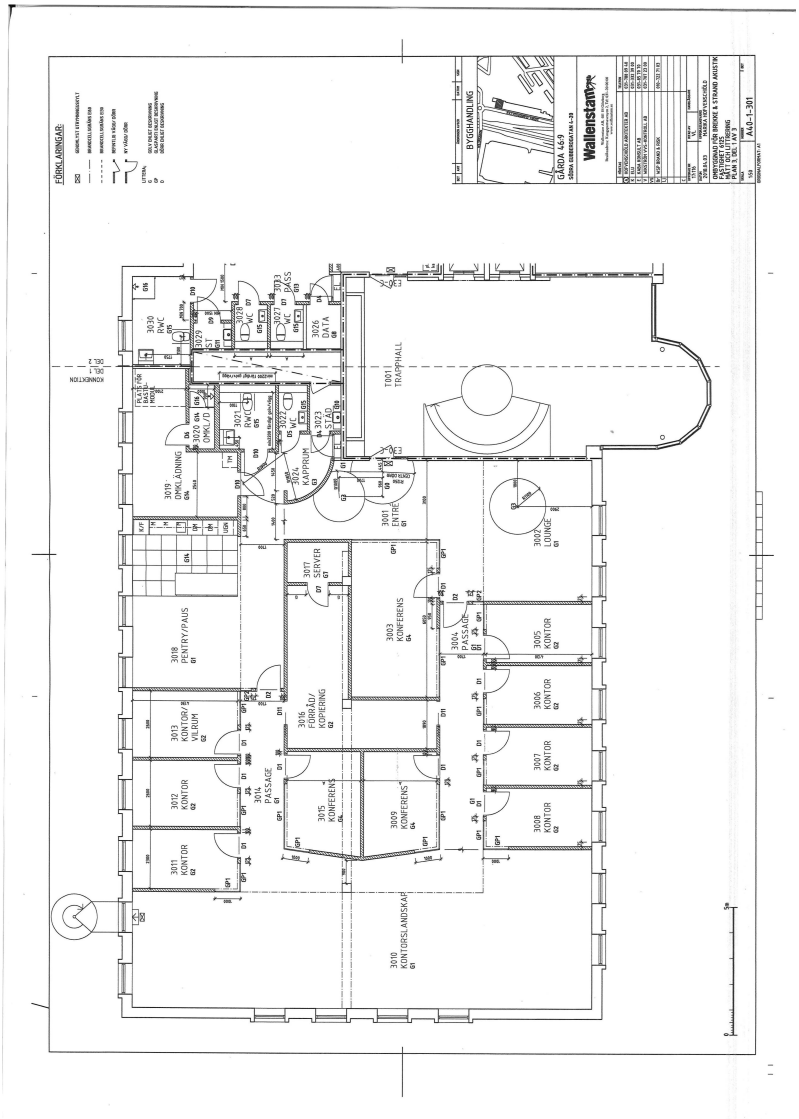

Figure A.1: Floor plan.

A.2 List of Equipment

No.	Name	Model
1	Kettlebell	12 kg
2	Accelerometer (pt. 1)	PCB single axis ICP, model 333B40, serial no. 70718
3	Accelerometer (pt. 2)	PCB Triaxial ICP, model 356B18, serial no. LW287516
4	Accelerometer (pt. 3)	PCB Triaxial ICP, model 356B18, serial no. LW287515
5	Accelerometer (pt. 4)	PCB single axis ICP, model 333B40, serial no. 70717
6	SQuadriga III	Head Acoustics
7	Laptop	with ArtemiS SUITE software installed
8	Mat	15-mm thick soft rubber mat

Table A.1: List of Equipment.

B

Appendix 2

MATLAB codes are available upon request. Please contact the author via email: `mailto:jiali.cheng@outlook.com`.

B.1 Spectrograms

B.1.1 Excitation Floor A

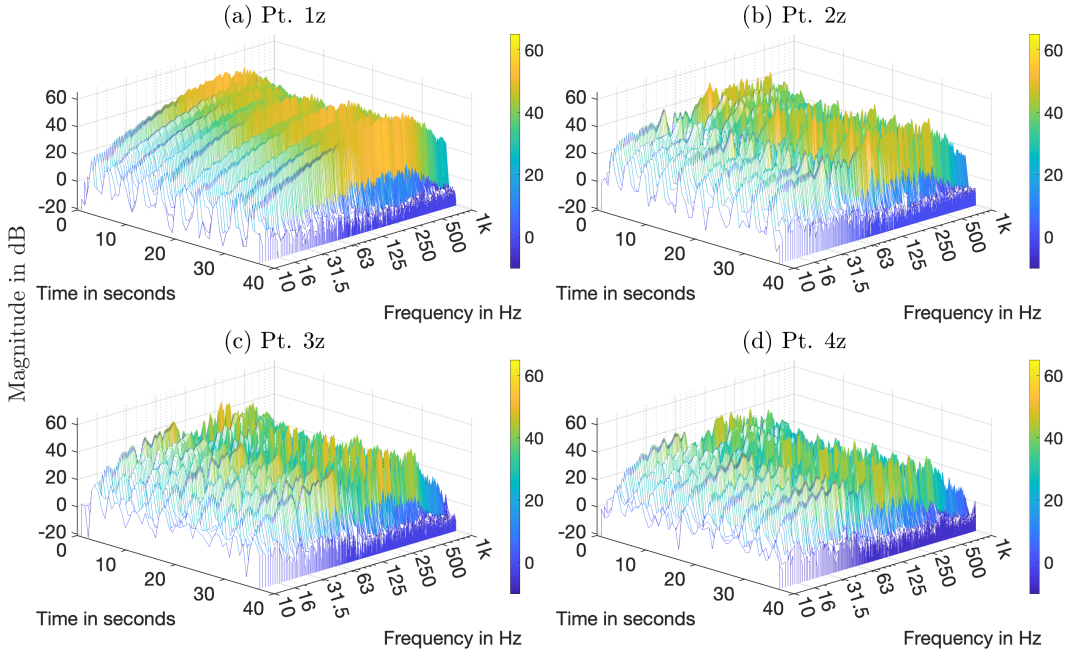

Figure B.1: Spectrogram of acceleration at position (a) pt. 1, (b) pt. 2, (c) pt. 3, and (d) pt. 4, excited at position Floor A.

B.1.2 Excitation Floor B

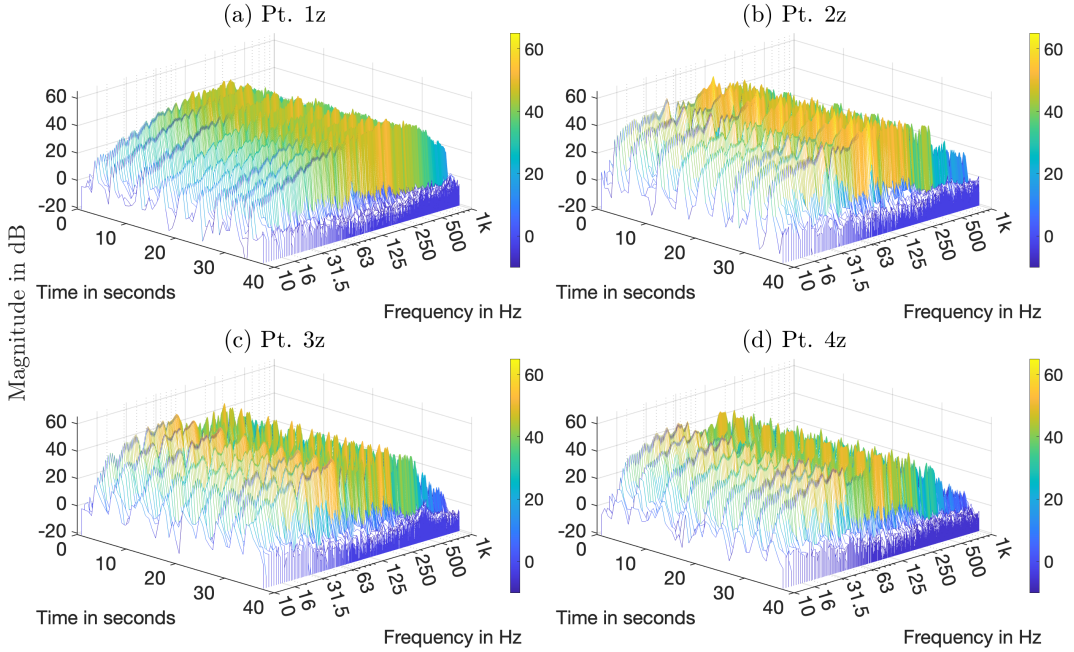

Figure B.2: Spectrogram of acceleration at position (a) pt. 1, (b) pt. 2, (c) pt. 3, and (d) pt. 4, excited at position Floor B.

B.1.3 Excitation Floor C

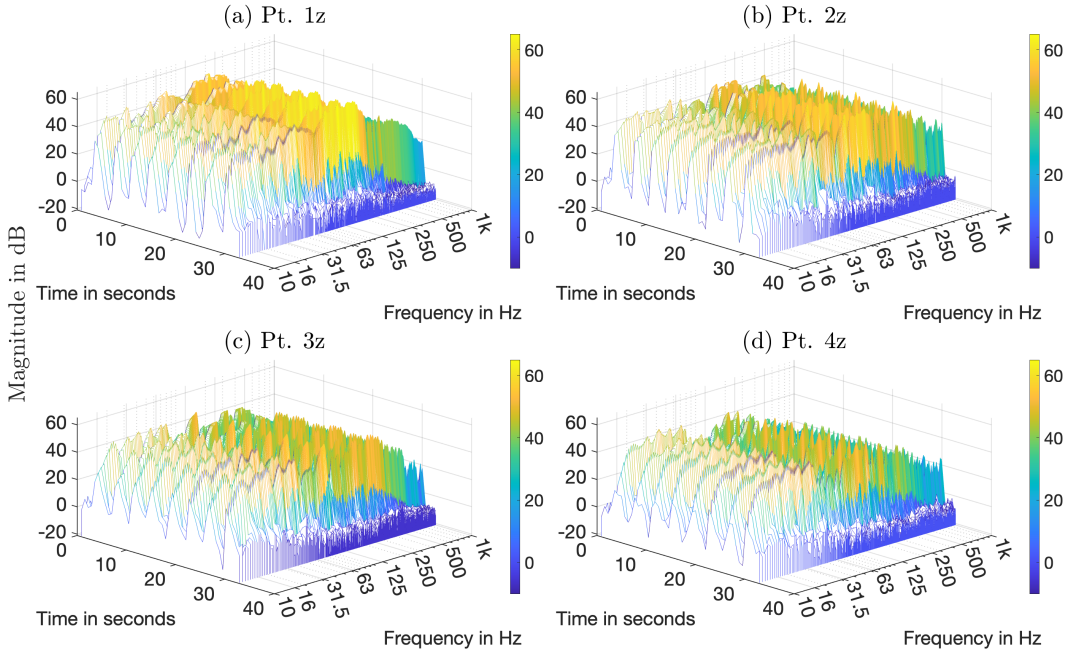

Figure B.3: Spectrogram of acceleration at position (a) pt. 1, (b) pt. 2, (c) pt. 3, and (d) pt. 4, excited at position Floor C.

B.1.4 Excitation Wall D

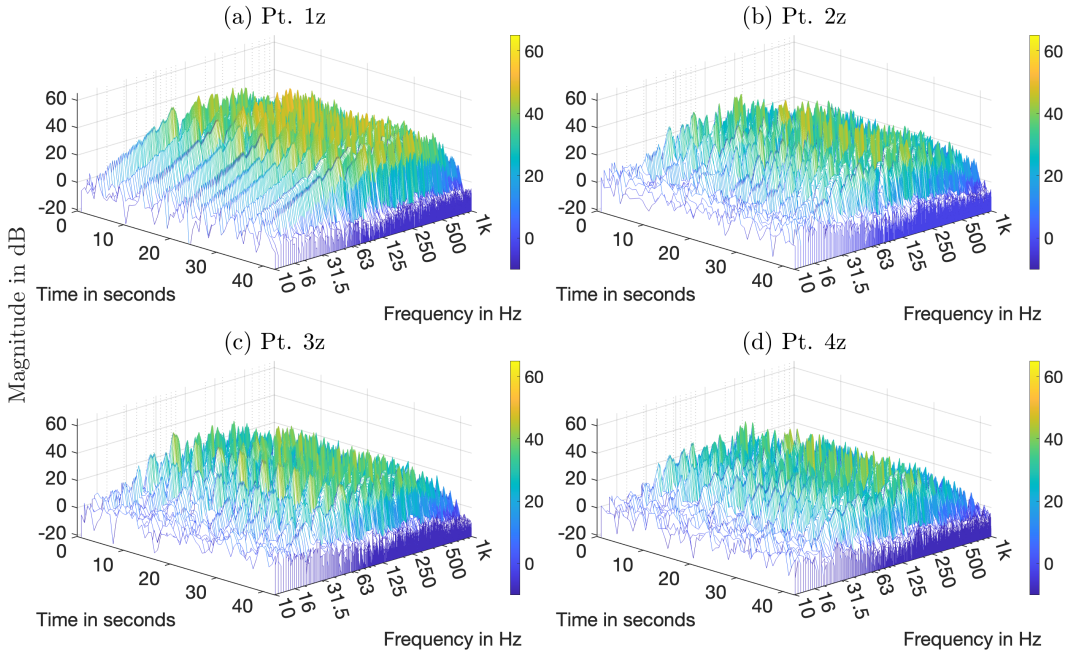

Figure B.4: Spectrogram of acceleration at position (a) pt. 1, (b) pt. 2, (c) pt. 3, and (d) pt. 4, excited at position Wall D.

B.2 Time Delay & Propagation Speed

B.2.1 Excitation Floor A

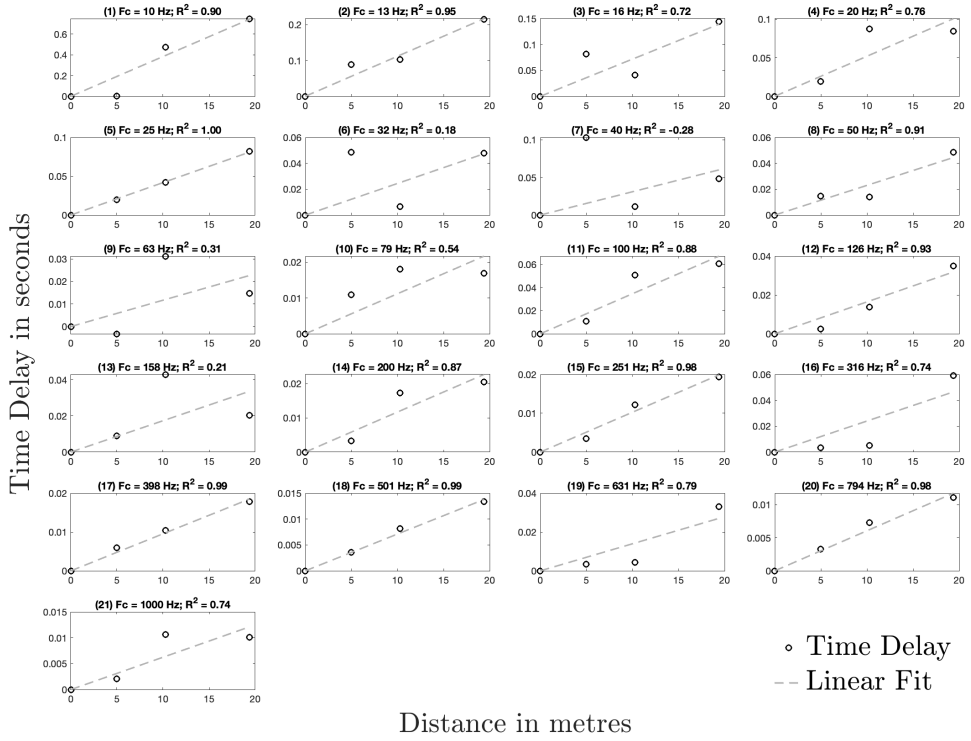

Figure B.5: Time delay of the acceleration at measurement positions reference to Point 1, excited at position Floor A.

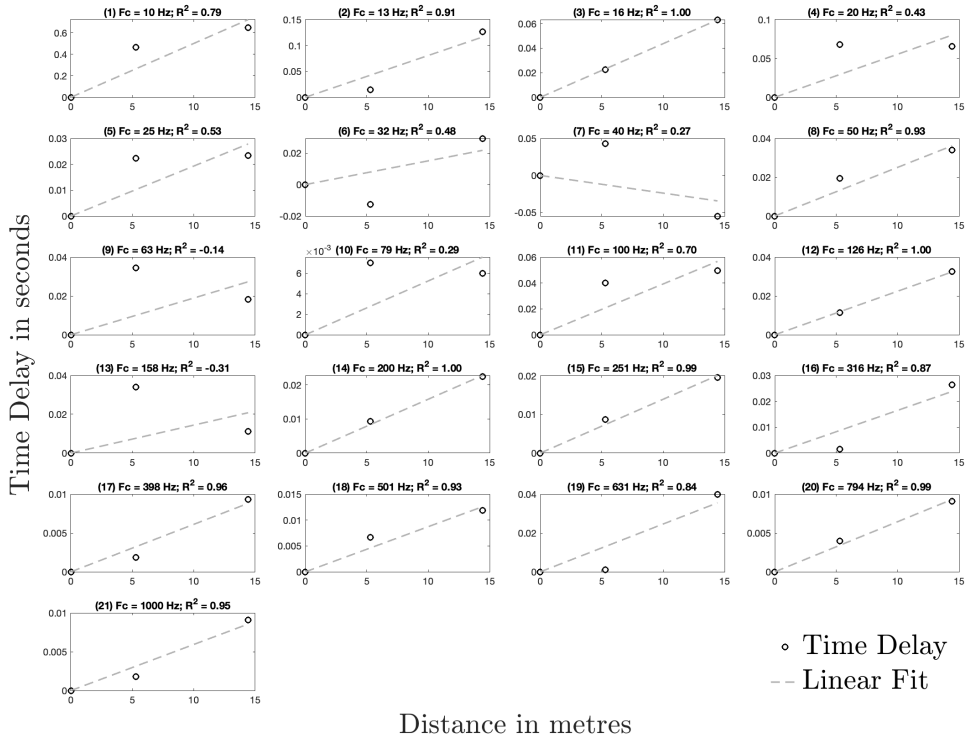

Figure B.6: Time delay of the acceleration at measurement positions reference to Point 2, excited at position Floor A.

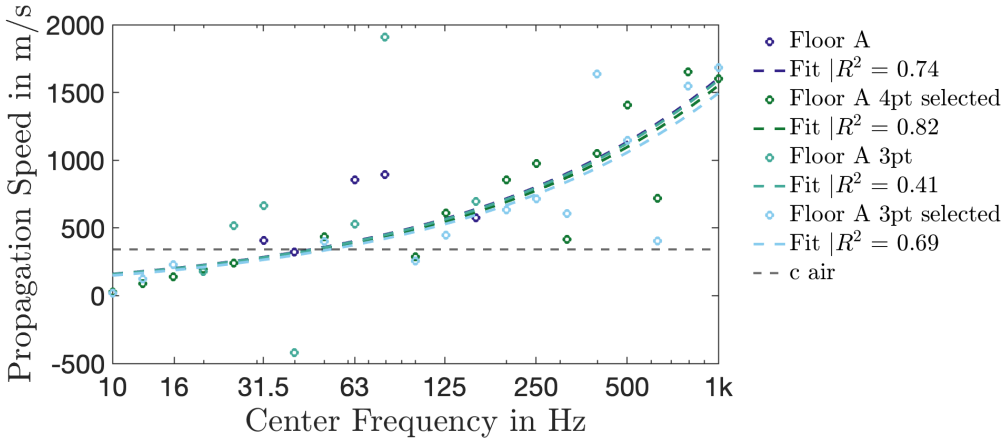

Figure B.7: Propagation speed of the acceleration at measurement positions reference to Point 1 and Point 2, excited at position Floor A.

B.2.2 Excitation Floor B

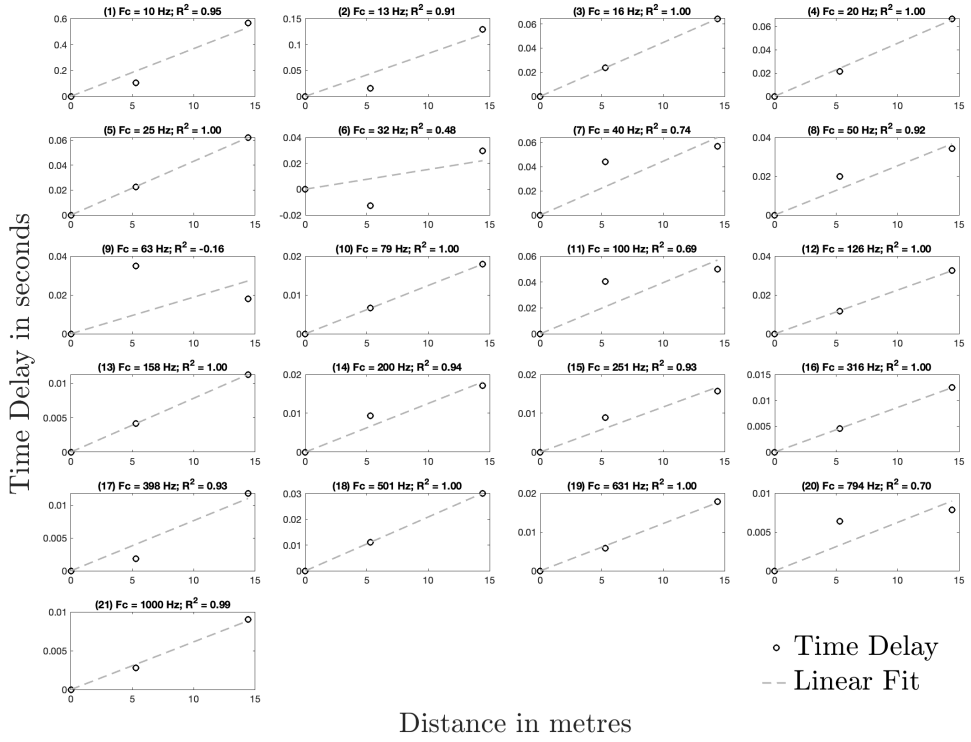

Figure B.8: Time delay of the acceleration at measurement positions reference to Point 2, excited at position Floor B.

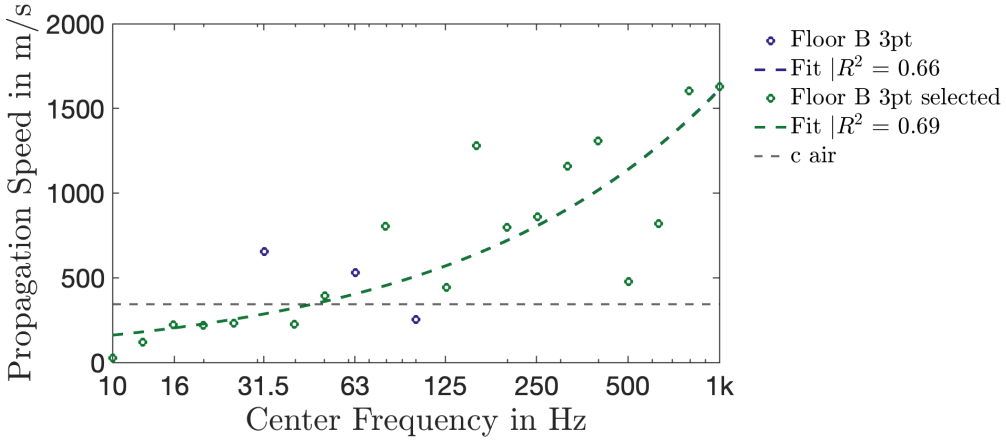

Figure B.9: Propagation speed the acceleration at measurement positions reference to Point 2, excited at position Floor B.

B.2.3 Excitation Floor C

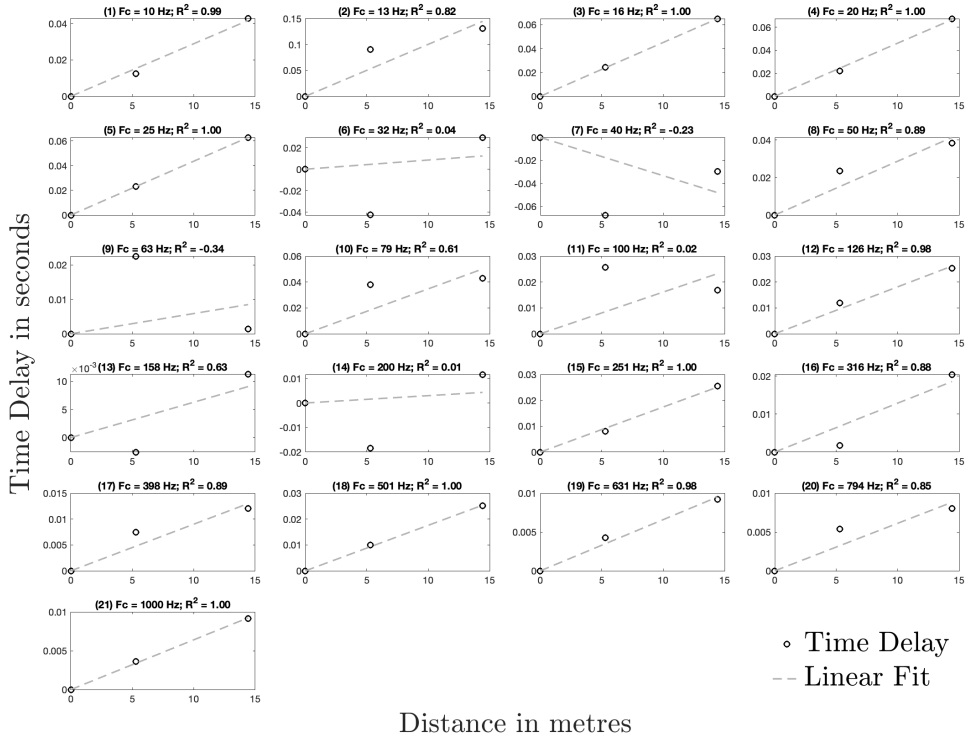

Figure B.10: Time delay of the acceleration at measurement positions reference to Point 2, excited at position Floor C.

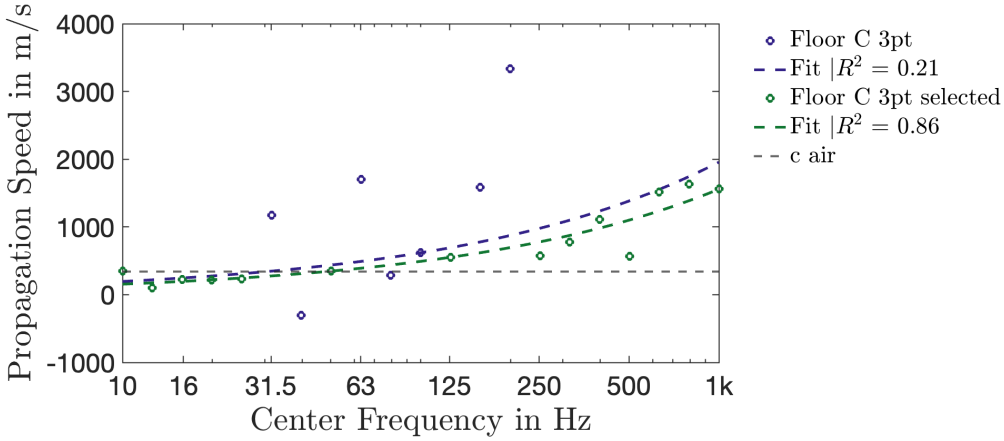

Figure B.11: Propagation speed of the acceleration at measurement positions reference to Point 2, excited at position Floor C.

B.2.4 Excitation Wall D

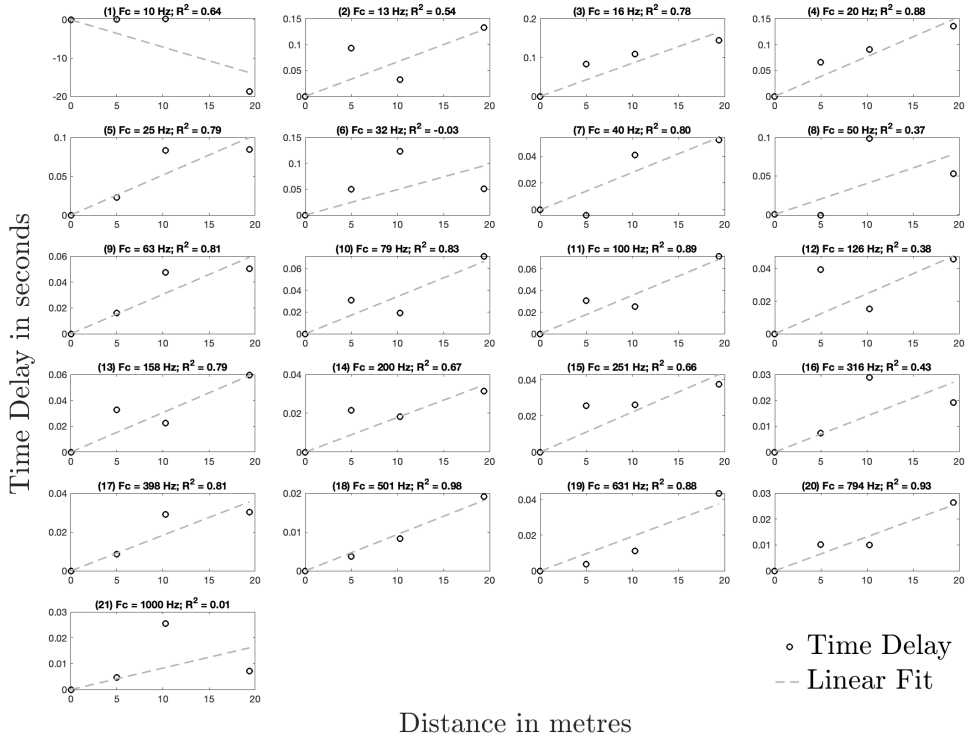

Figure B.12: Time delay of the acceleration at measurement positions reference to Point 1, excited at position Wall D.

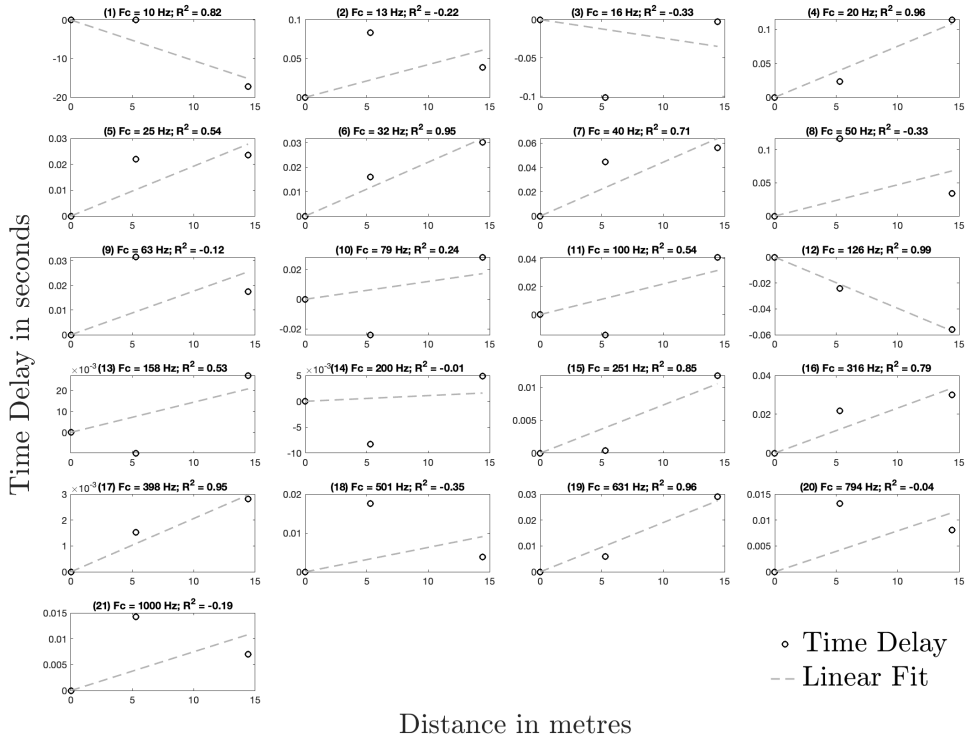

Figure B.13: Time delay of the acceleration at measurement positions reference to Point 2, excited at position Wall D.

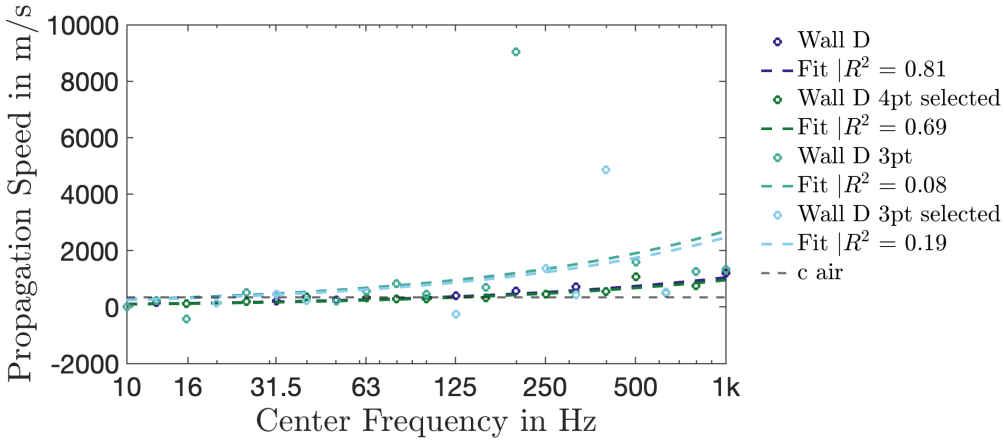

Figure B.14: Propagation speed of the acceleration at measurement positions reference to Point 1 and Point 2, excited at position Wall D.

B.3 Level Decay / Distance Attenuation

B.3.1 Excitation Floor A

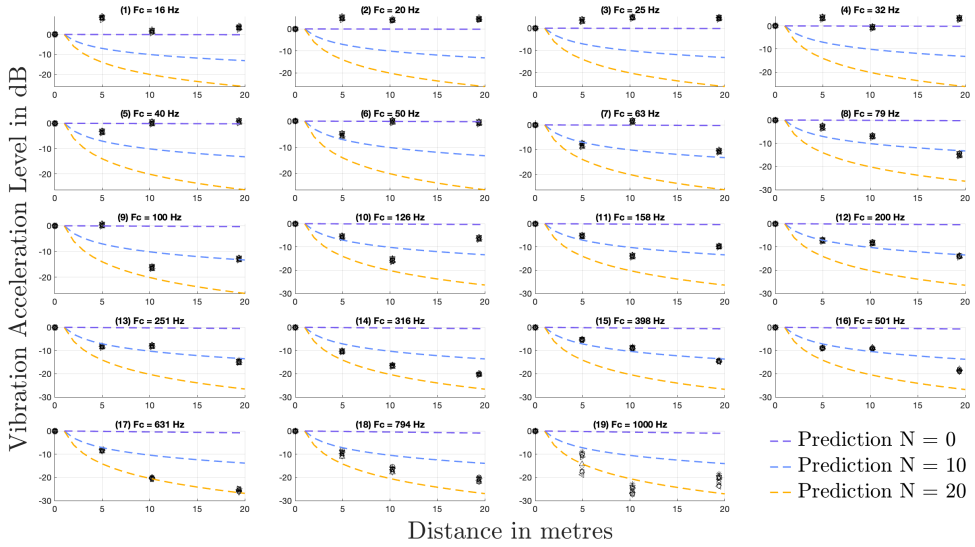

Figure B.15: Vibration acceleration level at measurement positions reference to pt. 1, excited at position Floor A.

B.4 Structural Reverberation Time

Structural reverberation time computations for each impulse response are available upon request due to the excessive number of plots.

B.5 Effective Speed

B.5.1 Propagation Speed

The propagation speed was computed based on centre time (centre of gravity time) and compared with that calculated based on time delay.

B.5.1.1 Excitation Floor A

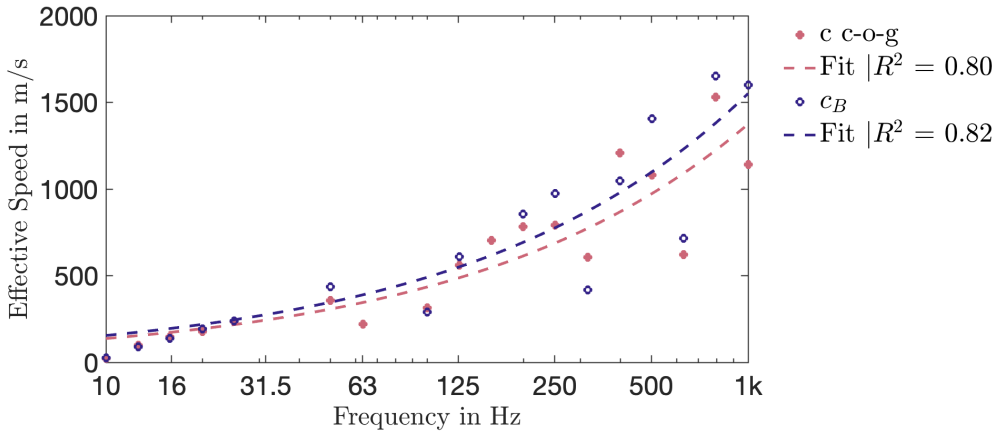

Figure B.16: Propagation speed based on centre time includes Point 1, excited at position Floor A.

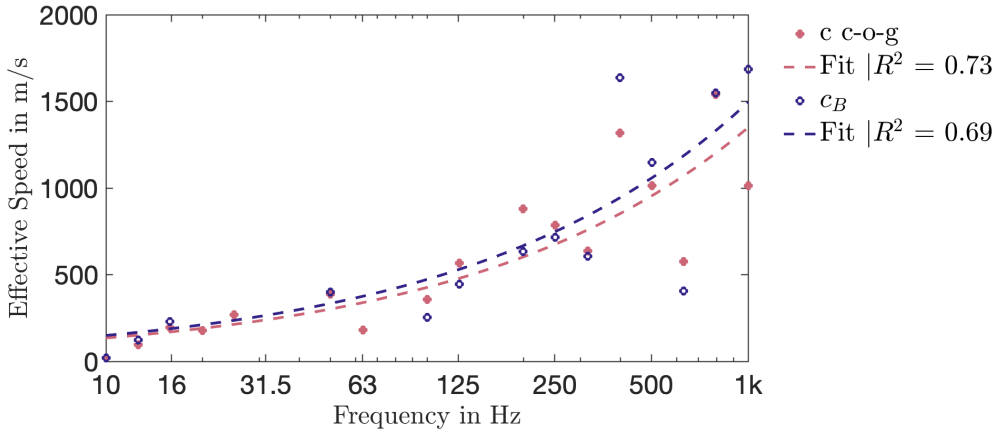

Figure B.17: Propagation speed based on centre time excluding Point 1, excited at position Floor A.

B.5.1.2 Excitation Floor B

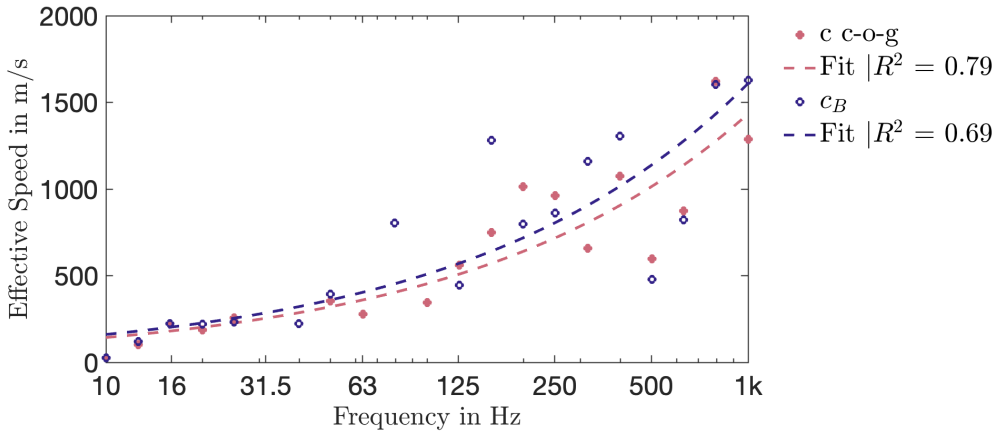

Figure B.18: Propagation speed based on centre time, excited at position Floor B.

B.5.1.3 Excitation Floor C

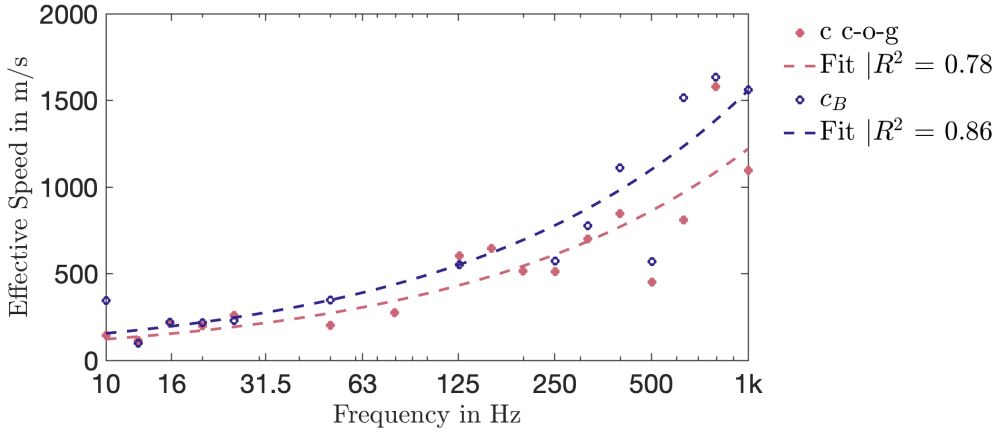

Figure B.19: Propagation speed based on centre time, excited at position Floor C.

B.5.2 Level Decay / Distance Attenuation

B.5.2.1 Excitation Floor C

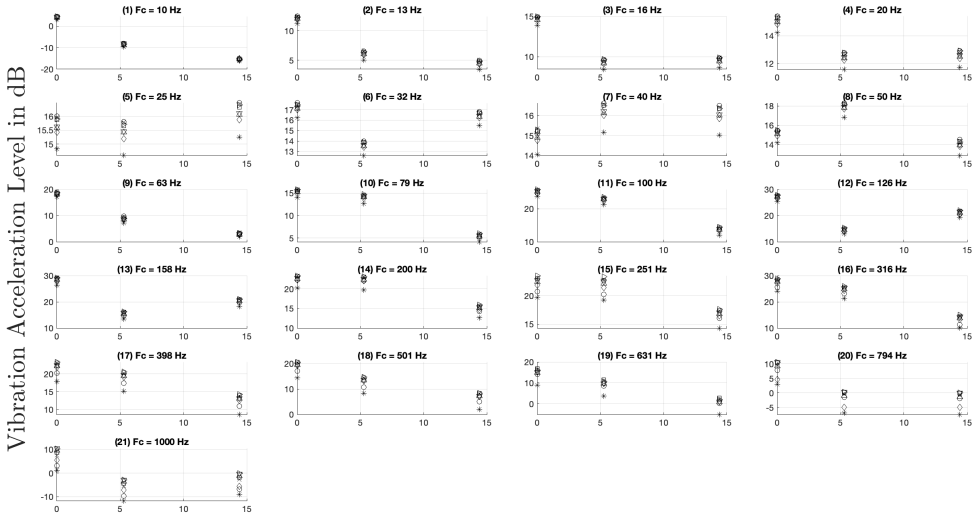

Figure B.20: Vibration acceleration level, excited at position Floor C.

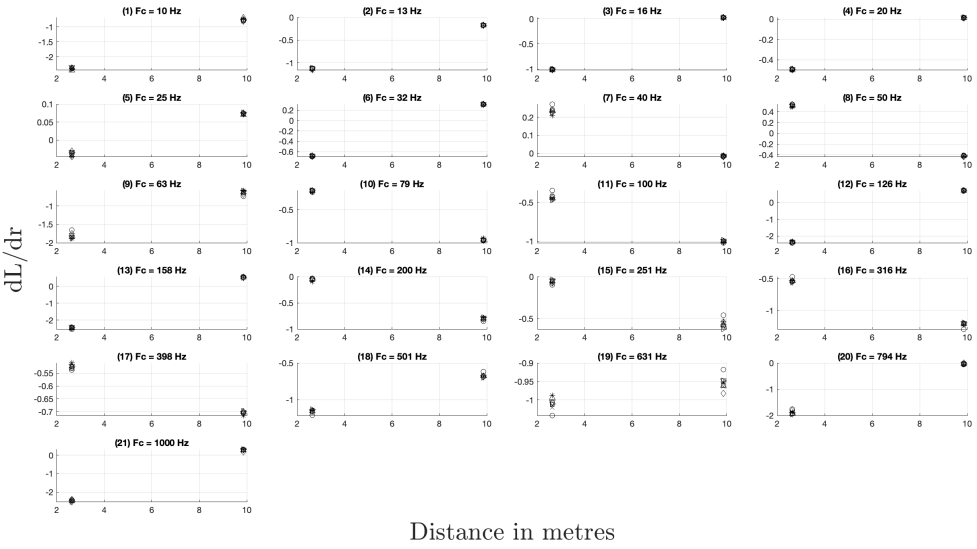

Figure B.21: dL/dr, excited at position Floor C.

B.5.3 Effective Speed

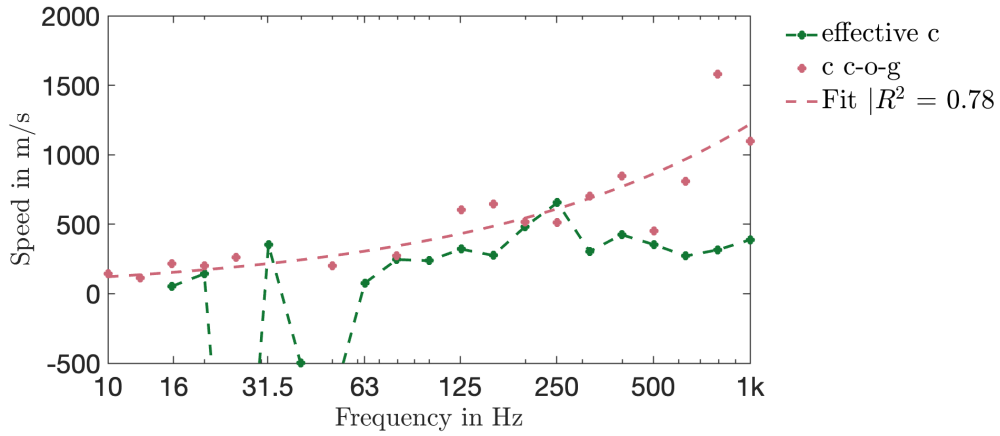

Figure B.22: Effective speed based on the ratio of $(dL/dt)/(dL/dr)$, compared with the propagation speed computed from the centre time (centre of gravity time). Excited at position Floor C.

DEPARTMENT OF SOME SUBJECT OR TECHNOLOGY
CHALMERS UNIVERSITY OF TECHNOLOGY
Gothenburg, Sweden
www.chalmers.se

CHALMERS
UNIVERSITY OF TECHNOLOGY